Дираковские фермионы и поверхностные состояния в полупроводниках и полуметаллах

В.А. Волков

ИРЭ им. В.А.Котельникова РАН, Москва

Сотрудничество:

И.В. Загороднев, В.В. Еналдиев, Ю.И. Латышев

«Идеи и методы физики конденсированного состояния» , Сочи, «Буревестник», 11-20 сентября 2015

Самая знаменитая формула в физике: «е равно эм ц квадрат».

**Точнее,
энергия релятивистского электрона (фермиона) корневым образом зависит от импульса (А. Эйнштейн):**

$$E = \pm\sqrt{m^2c^4 + p^2c^2}$$

В покое: $E = \pm mc^2$

Безмассовая частица: $E =$ ï pc

Дираковские фермионы: настоящие и эффективные (в полупроводниках)

Дирак (1928 г.)
«*Массивные фермионы*»

$E^2 = p^2 + (mc)^2$

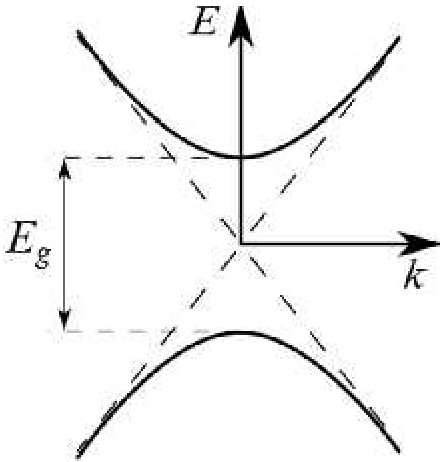

“Дираковские” кристаллы (Bi, PbTe и др.):
$E_g = 2mc^{*2}$ – *энергетическая щель*

Вейль (1929 г.)
«*Безмассовые фермионы*»

E = ï *pc*

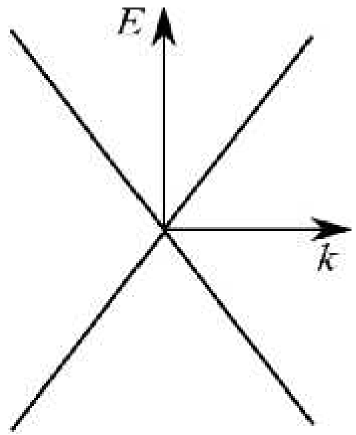

Графен:
c= c/300*
(*псевдо-релятивизм*!)

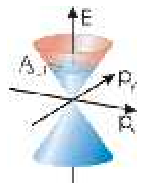

Various types of semimetals

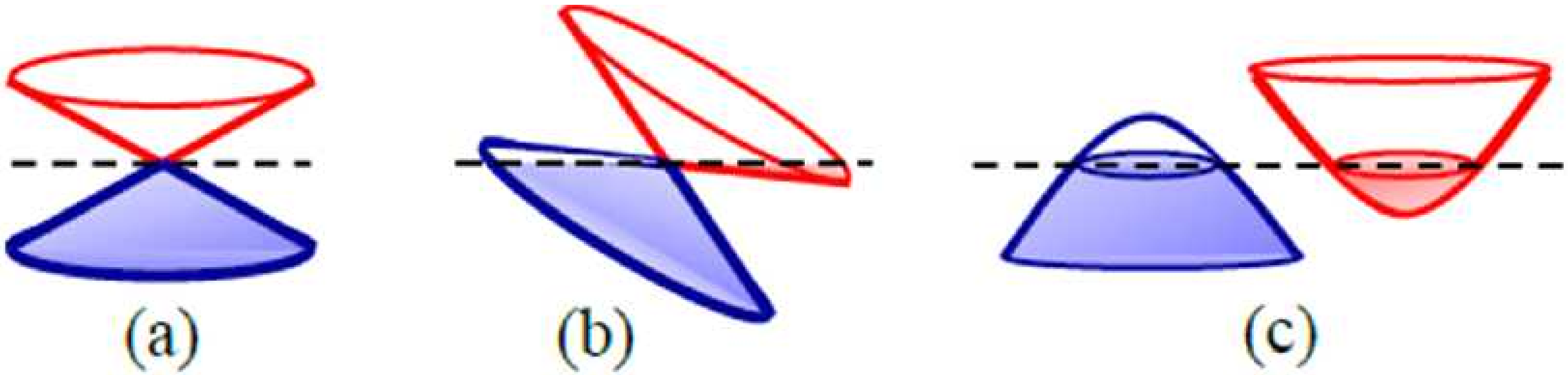

(a) Two conical bands that touch at a nodal point.
The Fermi surface is a point.
(b) Tilted cones (or type-II Weyl semimetal).
The Fermi surfaces enclose an electron pocket and a hole pocket.
(c) Overlapped bands that do not touch with each other.

Dashed lines denote the location of the chemical potential.

Hermann Weil (1929) and his Fermions (2015)

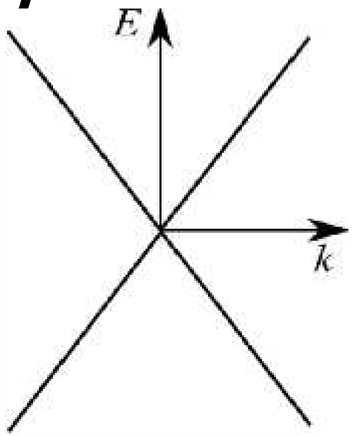

H. Weyl,
“Elektron und Gravitation. I,”
Z. Phys. 56, 330 (1929);

References

1. Wan, X. *et al. Phys. Rev. B* **83**, 205101 (2011).
2. Fu, L. *et al. Nature Photon.* **7**, 294–299 (2013).
3. Huang, S.-M. *et al. Nature Commun.* **6**, 7373 (2015). Theory
4. Weng, H. *et al. Phys. Rev. X* **5**, 011029 (2015).
5. Xu, S.-Y. *et al. Science* **349**, 613–617 (2015). Experiment
6. Lv, B. Q. *et al. Phys. Rev. X* **5**, 031013 (2015).
7. Lu, L. *et al. Science* **349**, 622–624 (2015).

Основы топологии

Топология отвечает на вопрос: можно ли *непрерывно преобразовать* один объект в другой?

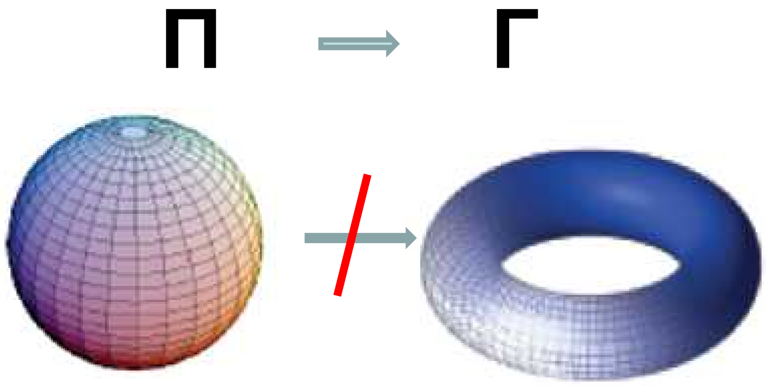

Одна из основных задач топологии:

найти математическую (топологическую) характеристику объекта (топологический инвариант).

Если объекты А и Б имеют разный топологический инвариант, то их нельзя непрерывно перевести друг в друга.

Topotronics

by Hasan group

- **Topo. Insulators & Berry's Phase**
- **Topo. Quant. Phase Transition**
- **Topo. Superconductors**
- **Topo. Crystalline Insulators**
- **Topo. Kondo Insulators**
- **Magnetic Topo. Insulators**
- **Dirac Semimetals**
- **Weyl Fermion Semimetals**
- **Majorana Heterostructures**
- **Natural Topo. Superconductors**

ПЛАН

- **Топология и твердое тело**
- **Краевые и поверхностные состояния**
- **Графен**
- **Топологические изоляторы**
- **Дираковские полуметаллы**
- **Вейлевские полуметаллы**
- ***Аксиальная аномалия***

Дираковские фермионы в графене

Пространственная и зонная структура графена

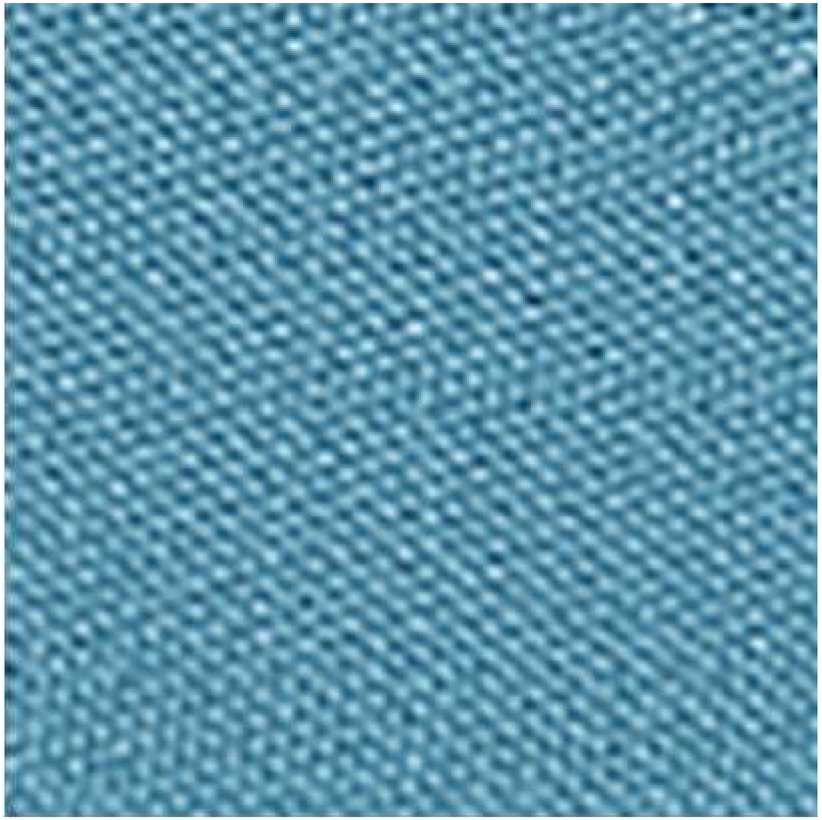

graphene lattice
in SuperSTEM

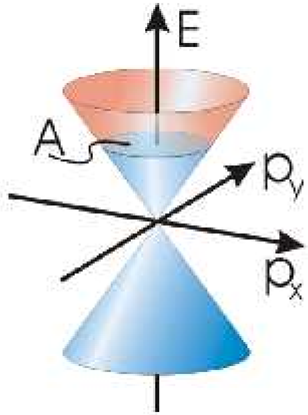

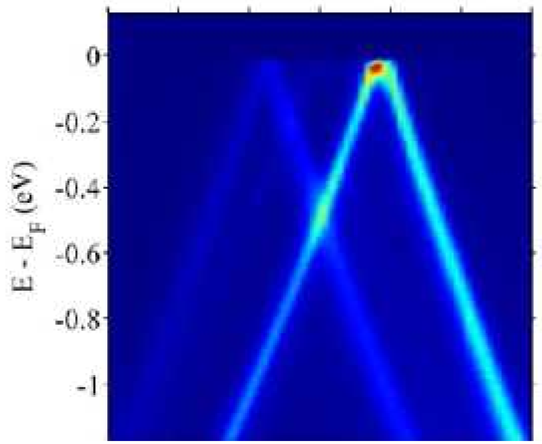

ARPES

Графеновый полевой транзистор: управление концентрацией и типом проводимости

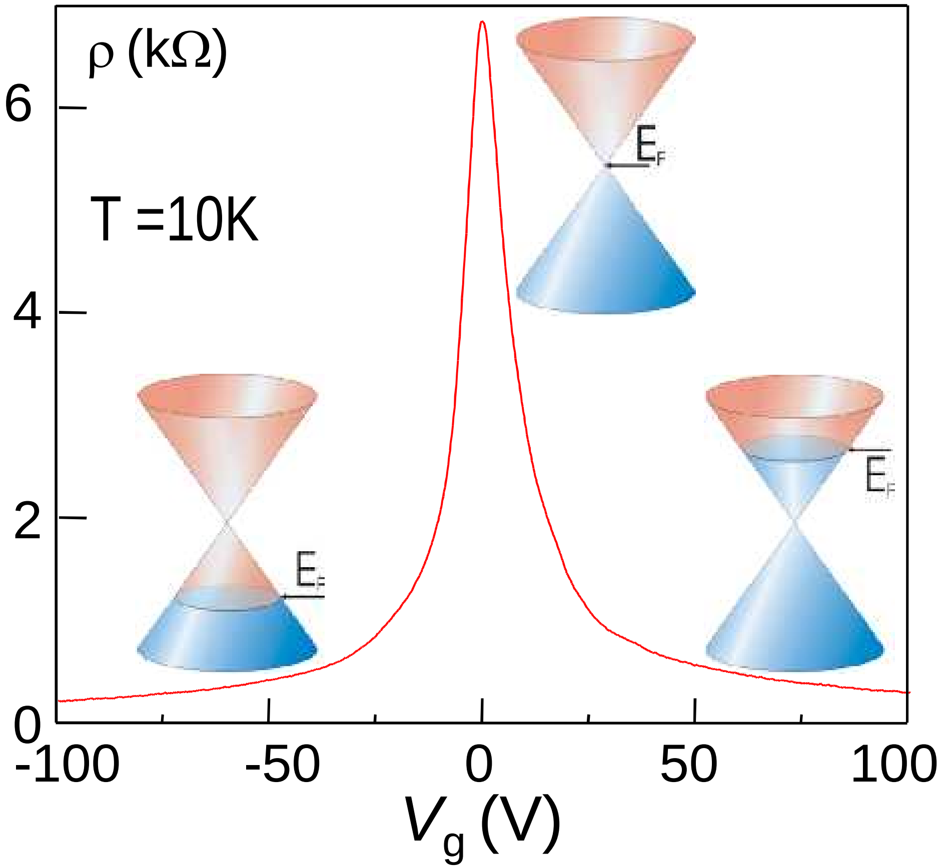

Первый полевой транзистор из полуметалла

Подвижность при 300 К:

20.000 см^2/В·с

(на порядок лучше, чем в кремнии)

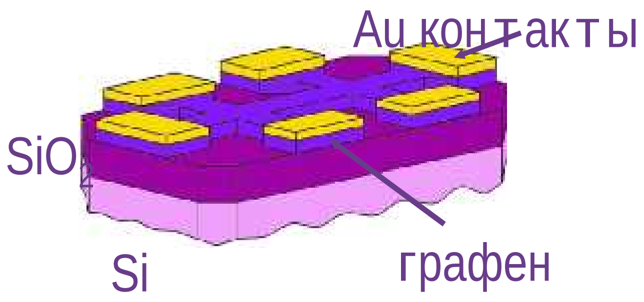

Novoselov et al, Science 2004

Краевые состояния Тамма-Дирака в наноперфорированном графене

Поверхностные состояния Тамма-Шокли

Полубесконечная решетка

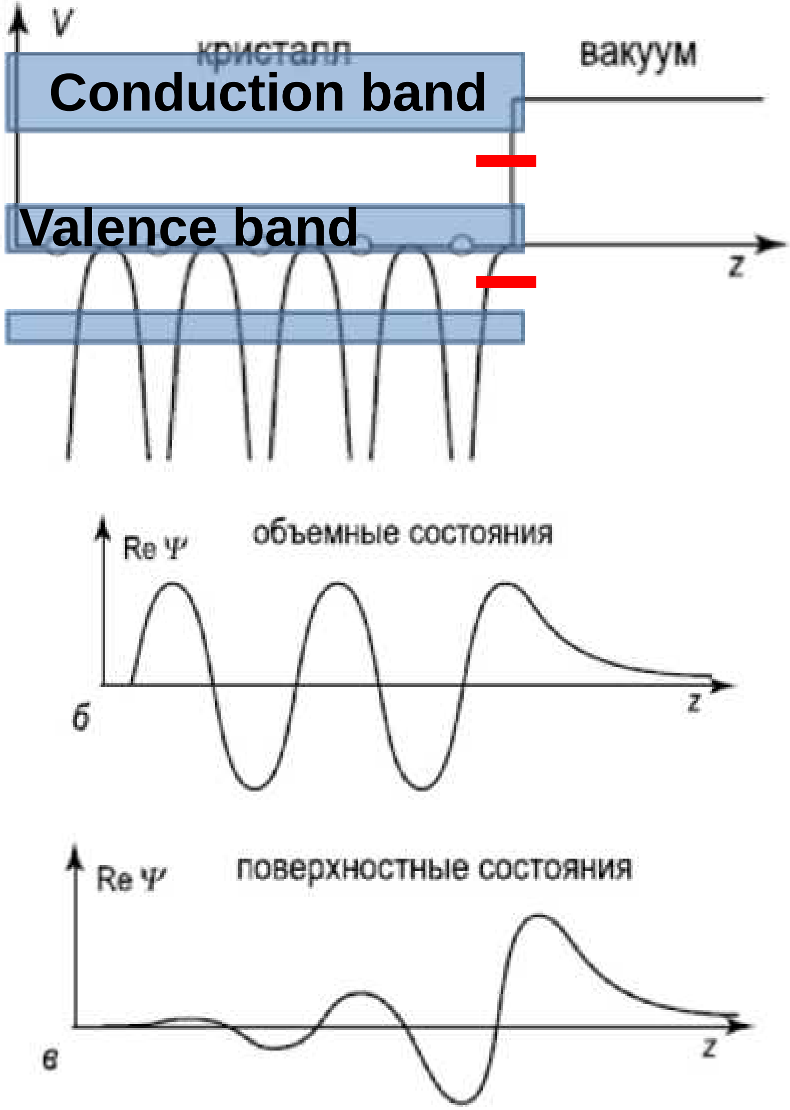

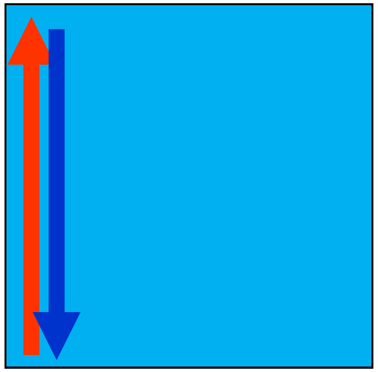

Краевые (таммовские) состояния в графене

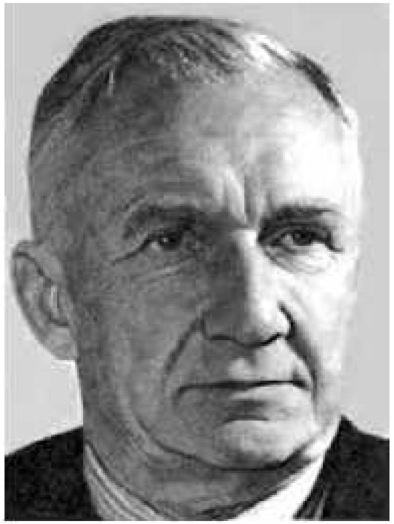

И.Е. Тамм, 1932

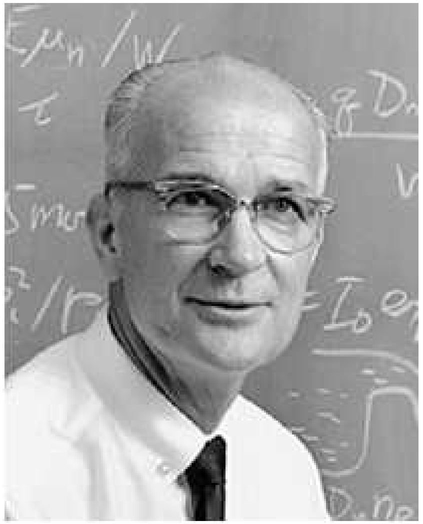

William Shockley, 1939

Nanohole in graphene: predicts of the theory of the edge Tamm-Dirac states

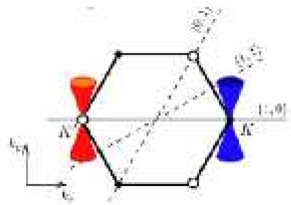

The edge states rotate around antidot for
both clockwise and counterclockwise circulations

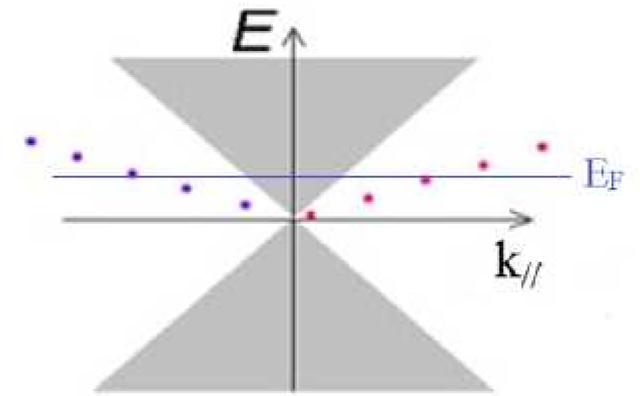

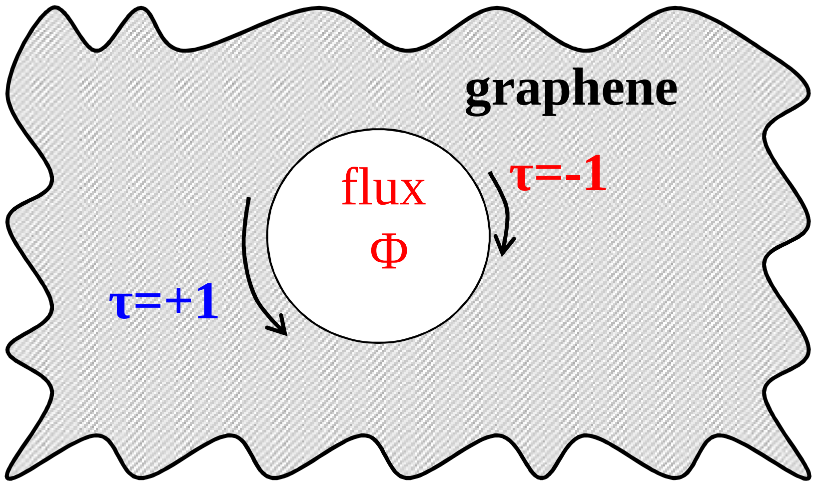

$$E_{2} R = {}^{2}\, 2va\left(j + \Phi / \Phi_0 - {}^{2} / 2 \right)$$

They experience the **orbital quantization**

$$k_{\parallel} = 2® \left(j - {}^{2} / 2 \right) / 2® R$$

$$j = \pm 1/2, \pm 3/2, \pm 5/2, \ldots$$

Φ/Φ_0 – the number of magnetic flux quanta through the antidot.

$\Phi = ® H R_0^2$

Yu.I. Latyshev et al (2014)

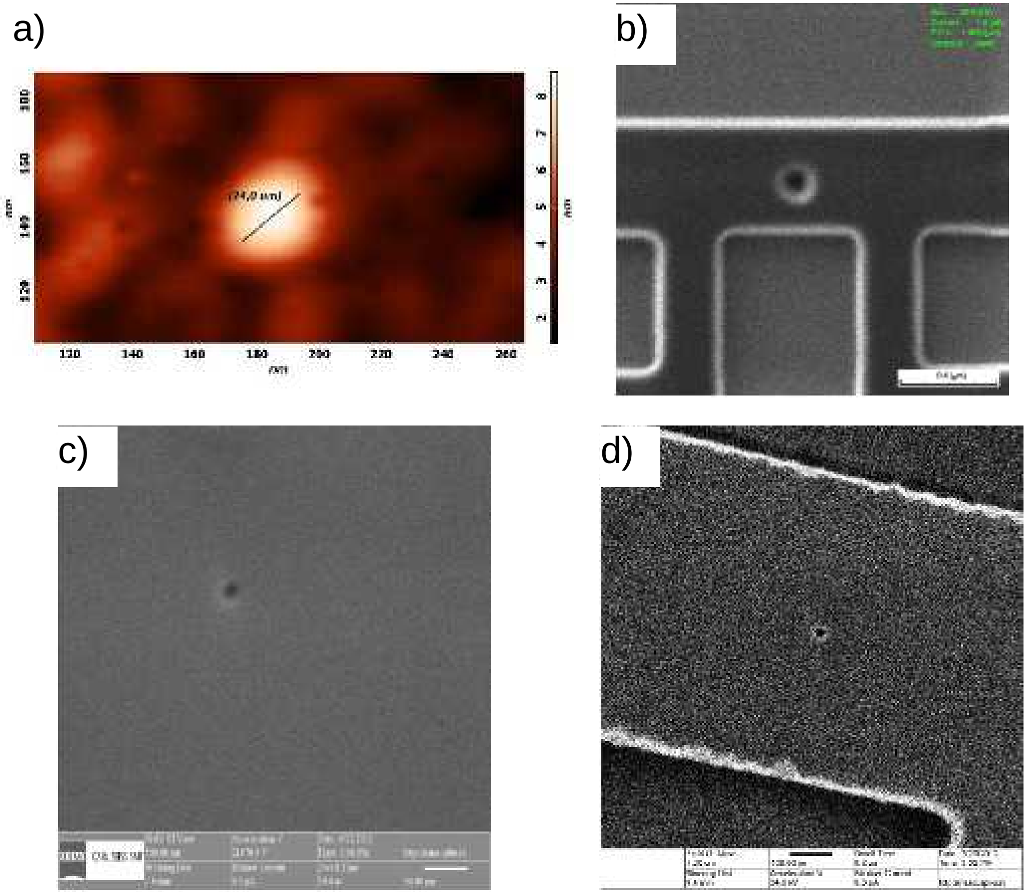

Experimental realization of graphene nanohole structures

a, Single holes produced by heavy ion irradiation (AFM image),
b, by FIB (SEM image) and
c, by helium ion microscope (SHIM image) on graphene (**c)** and
thin graphite (**a, b, d**).

Полевой транзистор на перфорированном графене

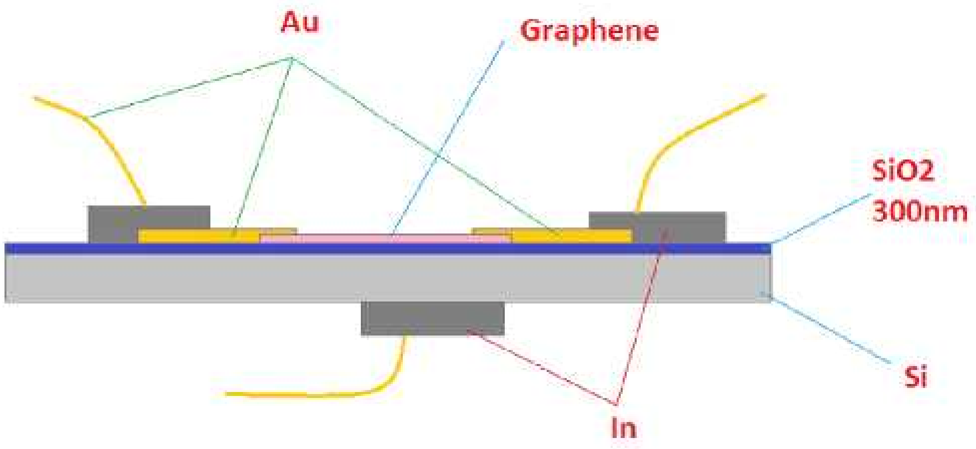

FET - structure with the back gate

SAMPLES
Nano-perforated graphene

1) Irradiation with heavy ions Xe^{+26} with energy of 170 МэВ, and fluence of 3 10^9 $см^{-2}$. Estimation of diameter of antidots (SEM, AFM) gives D=10 нм.

1) Irradiation with a focused helium ion beam on ion helium microscope ORION. Estimate: D=2 нм.

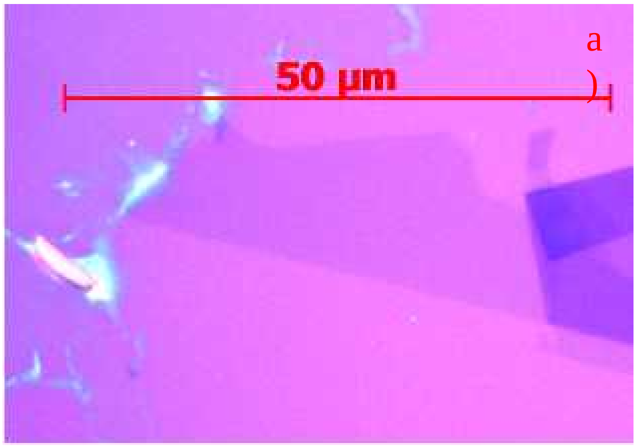

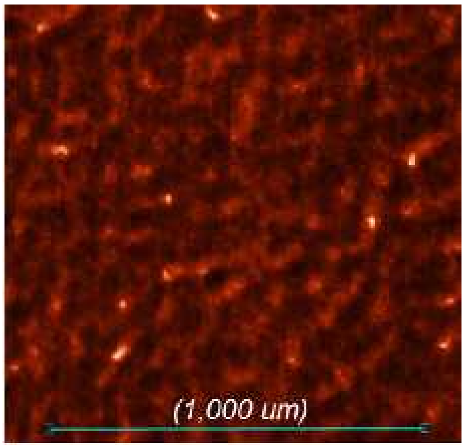

Осцилляции сопротивления перфорированного графена при изменении уровня Ферми; B = 0

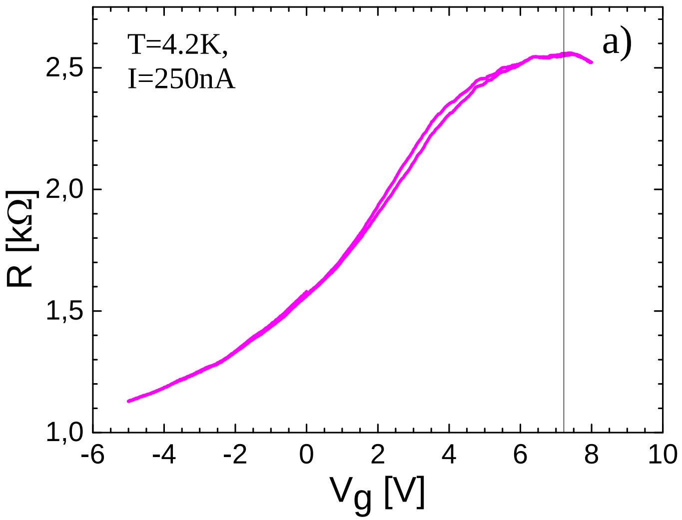

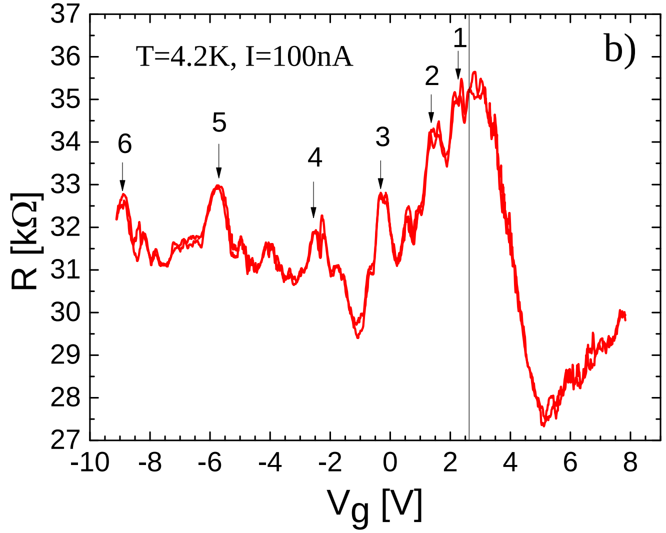

Зависимость сопротивления от затворного напряжения:

(a) - контрольный образец графена,

(b) - графен, облученный тяжелыми ионами

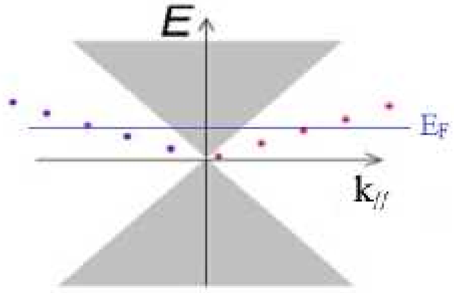

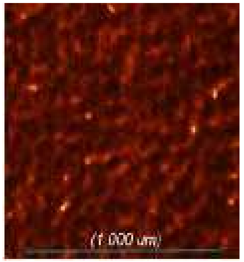

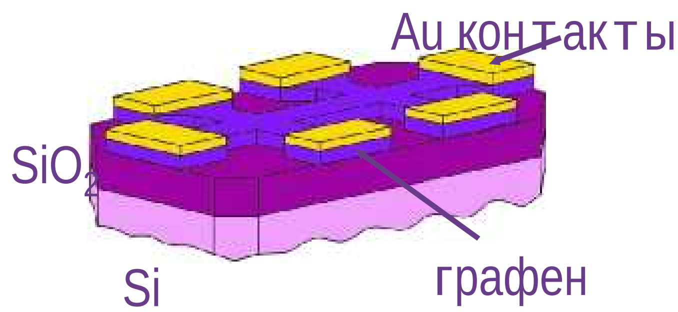

Single holes in nano-thin graphite (a, b) and graphene (c) produced

by FIB (D= 35 nm, SEM image)

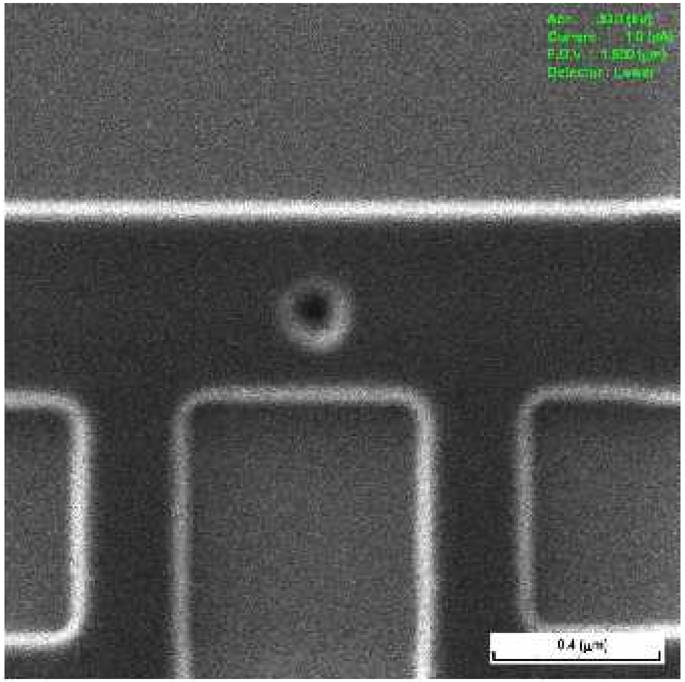

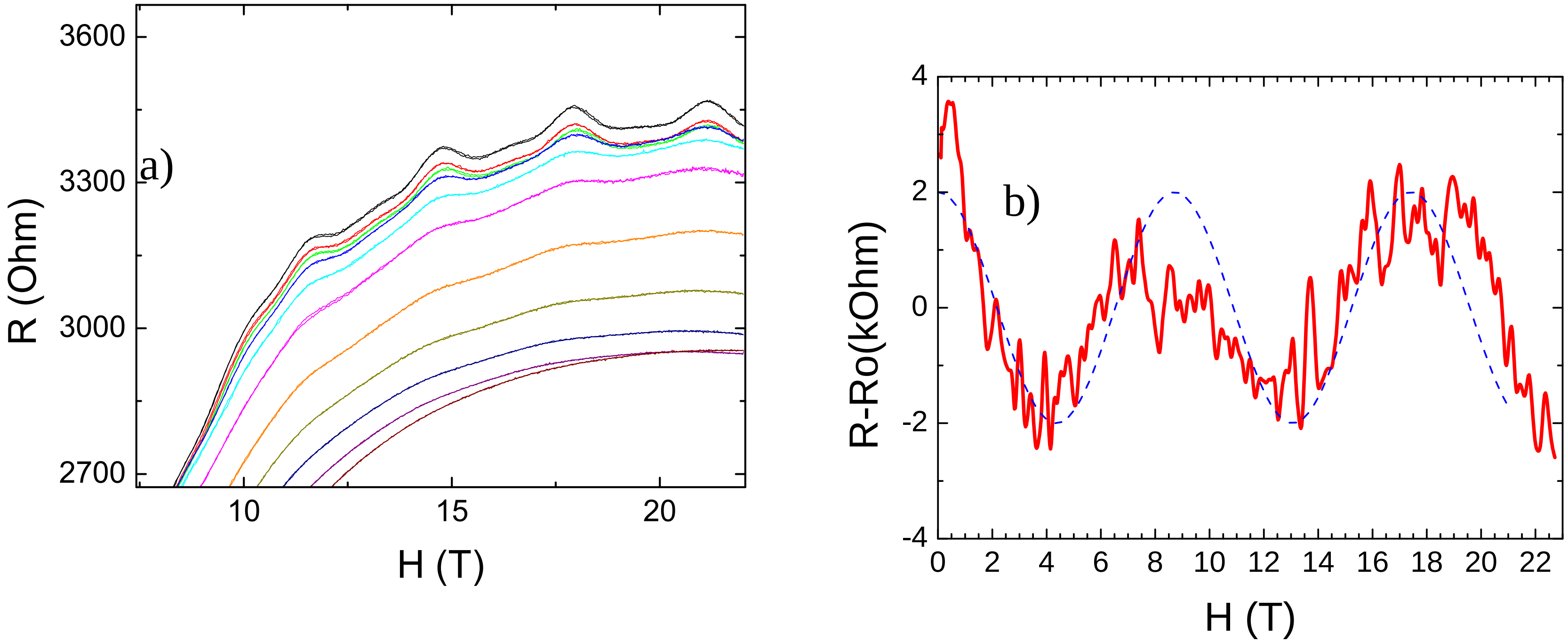

The Aharonov-Bohm resistance magneto-oscillations.
a. Field-periodic resistance oscillations for thin graphite single hole structure with FIB made nanohole with D= 37 nm ,
b, graphene structure with a single nanohole made by helium ion microscope, D=20 nm.

Yu.I. Latyshev, A.P. Orlov, V.A. Volkov, V.V. Enaldiev, I.V. Zagorodnev, O.F. Vyvenko, Yu.V. Petrov, P. Monceau.
“Transport of Massless Dirac Fermions in Non-topological Type Edge States”, Scientific Reports (December 19, 2014);

Результаты группы Ю. Латышева по графену

- Изготовлены образцы и исследован транспорт (эксперимент и теория) дираковских фермионов в наноперфорированных структурах на основе графена.
- Обнаружено орбитальное квантование краевых дираковских фермионов, вращающихся вокруг наноотверстий. Тем самым прямо доказано существование состояний Тамма-Шокли в графене
- С помощью измерений эффекта Ааронова-Бома в сопротивлении образцов прямым способом доказана проводящая природа состояний Тамма-Шокли в графене
- Из сравнения извлечен параметр теории. Он не зависит от технологии и характеризует усредненную вдоль траектории ДФ микроскопику краевого потенциала.

ТОПОЛОГИЧЕСКИЕ ИЗОЛЯТОРЫ

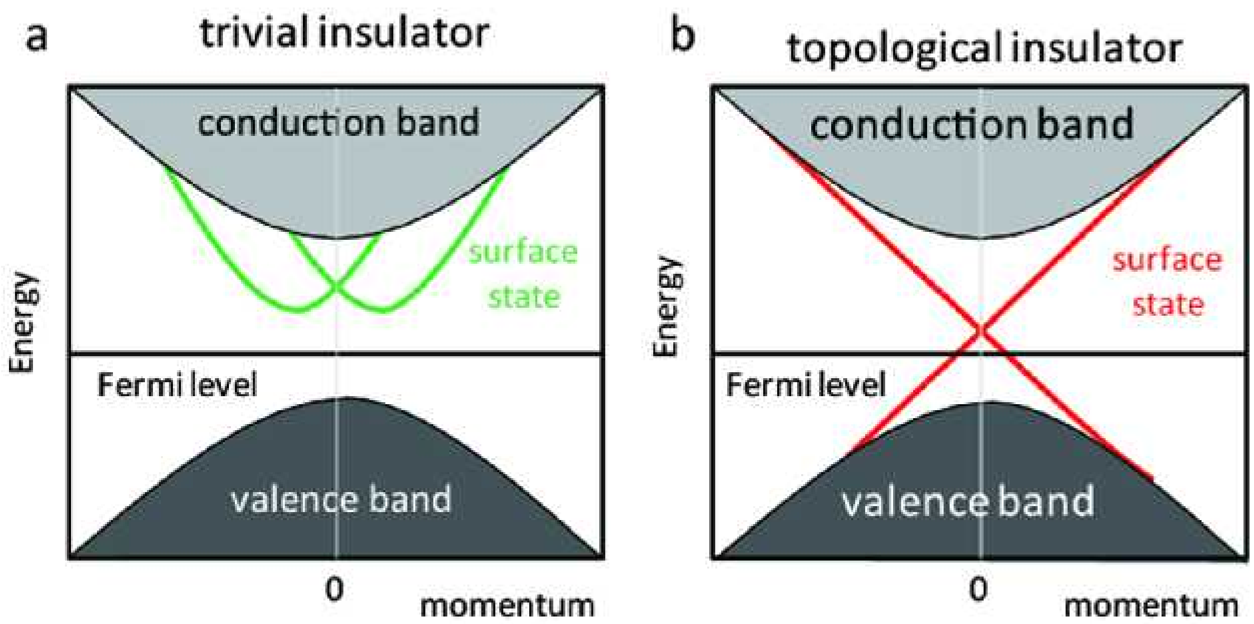
a
trivial insulator
b
topological insulator
conduction band
surface
state
Energy
Fermi level
valence band
0
momentum
conduction band
surface
state
Energy
Fermi level
valence band
0
momentum

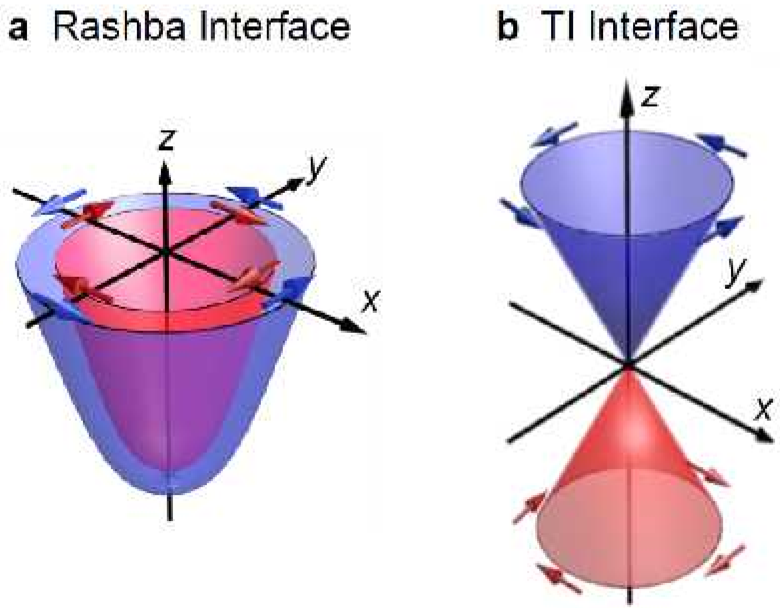
a Rashba Interface
b TI Interface
z
y
x
z
y
x

Topological Insulators and SSs

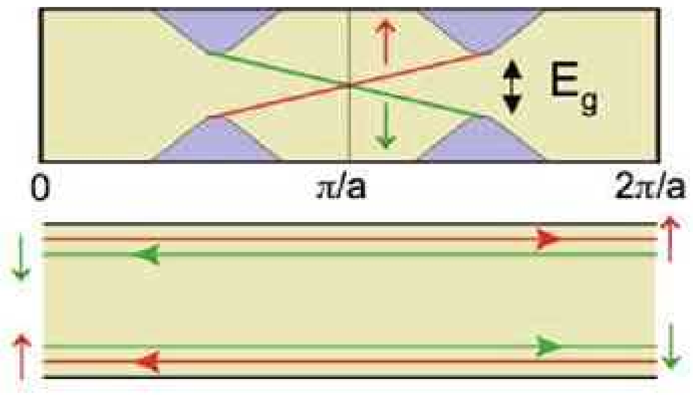

Topological Insulators

Topological insulators are insulating materials that conduct electricity on their surface via special surface electronic states;

- The surface states of topological insulators are topologically protected, which means that unlike ordinary surface states they cannot be destroyed by impurities or imperfections
- Topological insulators are made possible because of two features of quantum mechanics: symmetry under the reversal of the direction of time; and the spin–orbit interaction, which occurs in heavy elements such as mercury and bismuth
- The topological insulator states in 2D and 3D materials were predicted theoretically in 2005 and 2007, prior to their experimental discovery

2D and 3D TopoIns

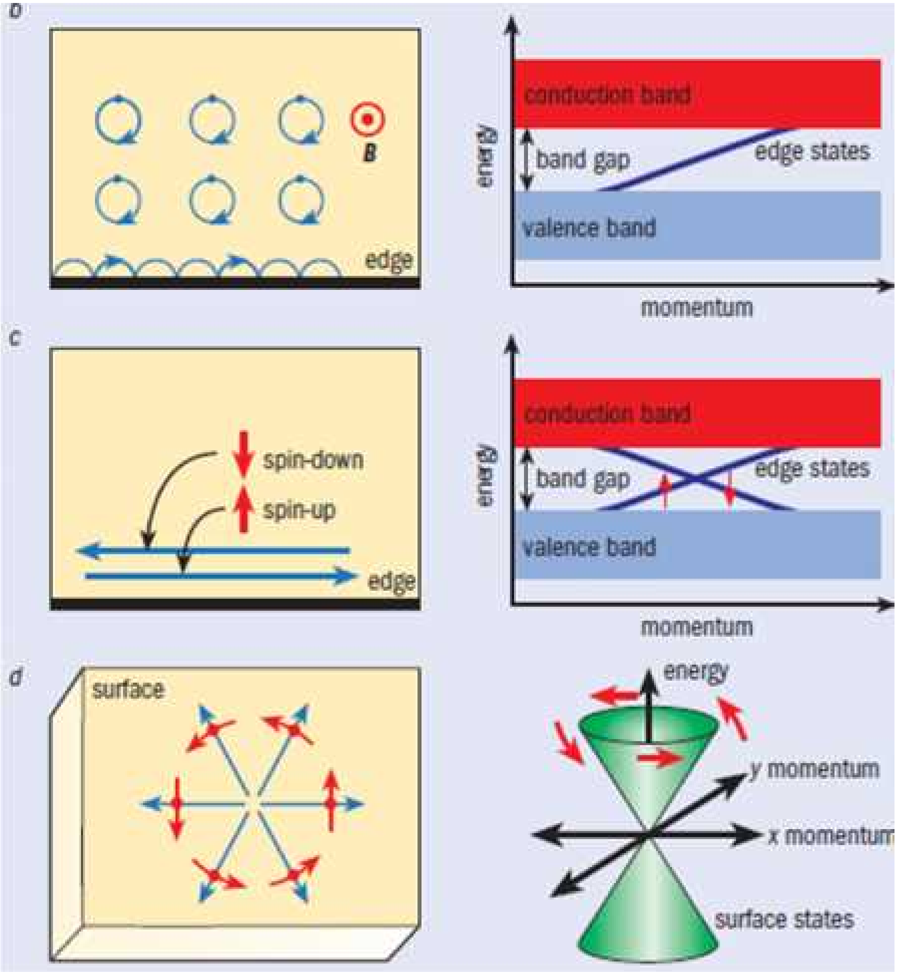

(*b*) The quantum Hall effect.
At the edge, electrons execute "skipping orbits", leading to perfect conduction in one direction along the edge.
(*c*) The edge of 2D topological insulator contains left-moving and right-moving modes that have opposite spin and are related by time-reversal symmetry.
(*d*) The surface of a 3D topological insulator supports motion in any direction along the surface, but the direction of the electron's motion uniquely determines its spin direction and vice versa. The 2D energy–momentum relation has a "Dirac cone" structure similar to that in graphene.

$Bi_{1-x}Sb_x$

Pure Bismuth	Alloy : $.09<x<.18$	Pure Antimony
semimetal	semiconductor E_{gap} ~ 30 meV	semimetal

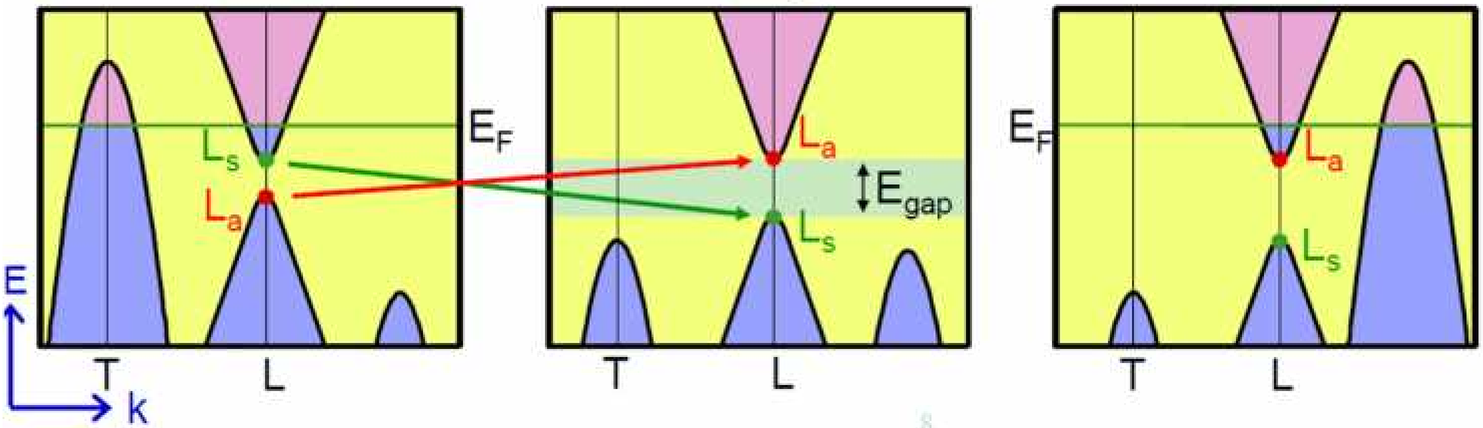

Inversion symmetry $\Rightarrow$ $(-1)^{\nu_0} = \prod_{i=1}^{8}\prod_n \xi_{2n}(\Gamma_i)$

Bismuth

1Γ	Γ_6^+	Γ_6^-	Γ_6^+	Γ_6^+	Γ_{45}^+	$-$
$3L$	L_s	L_a	L_s	L_a	L_a	$-$
$3X$	X_a	X_s	X_s	X_a	X_a	$-$
$1T$	T_6^-	T_6^+	T_6^-	T_6^+	T_{45}^-	$-$
	Z_2 class					$(0;000)$

Antimony

1Γ	Γ_6^+	Γ_6^-	Γ_6^+	Γ_6^+	Γ_{45}^+	$-$
$3L$	L_s	L_a	L_s	L_a	L_s	$+$
$3X$	X_a	X_s	X_s	X_a	X_a	$-$
$1T$	T_6^-	T_6^+	T_6^-	T_6^+	T_{45}^-	$-$
	Z_2 class					$(1;111)$

Predict $Bi_{1-x}Sb_x$ is a strong topological insulator: $(1\ ;\ 111)$.

Topological insulator bismuth calcium selenide

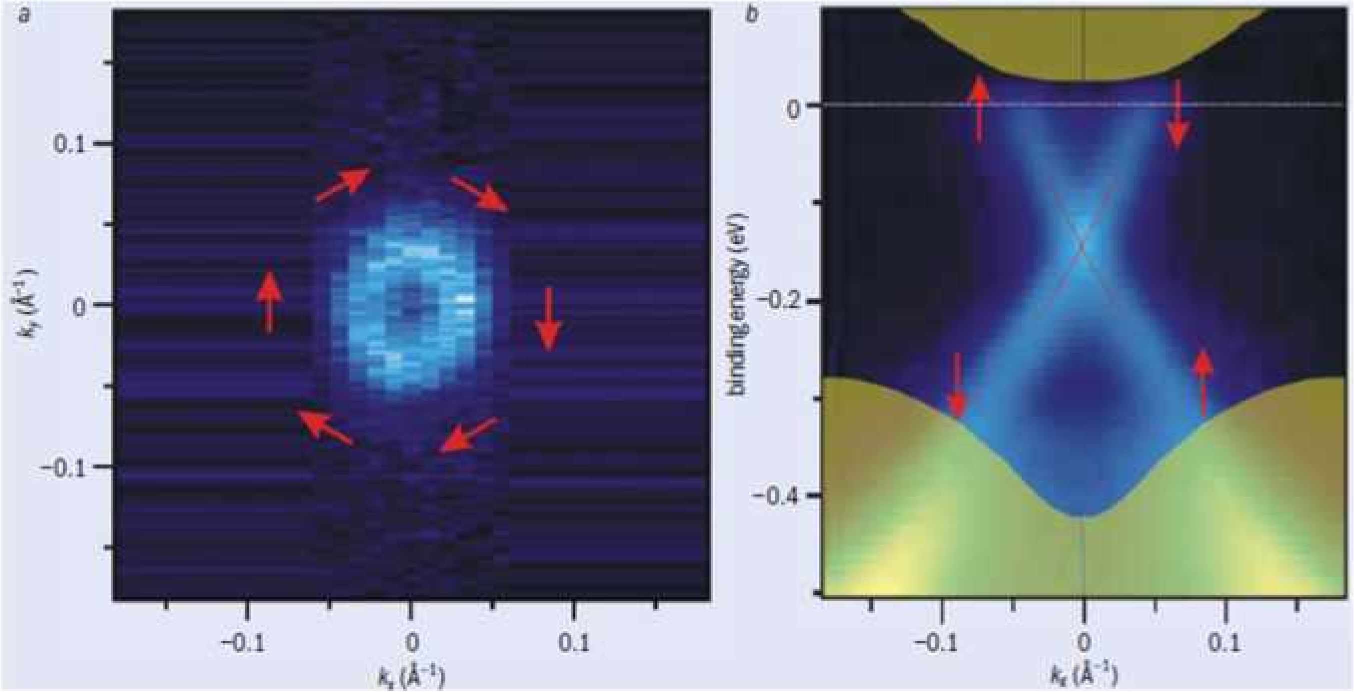

(*a*) Fermi-surface map for the surface of the topological insulator $Bi_{2-x}Ca_xSe_3$ measured by spin-resolved ARPES as a function of the surface momentum, k_x and k_y. The spin direction precesses with electron momentum around the circular Fermi surface, and opposite momenta have opposite spin. (*b*) The surface bands intersect at a “Dirac point” marked by the cross that is inside the bulk band gap at approximately 0.25 eV. The calcium concentration, x, is tuned so that the Fermi energy lies between the bulk valence and conduction bands.

3D топологический изолятор Bi_2Se_3

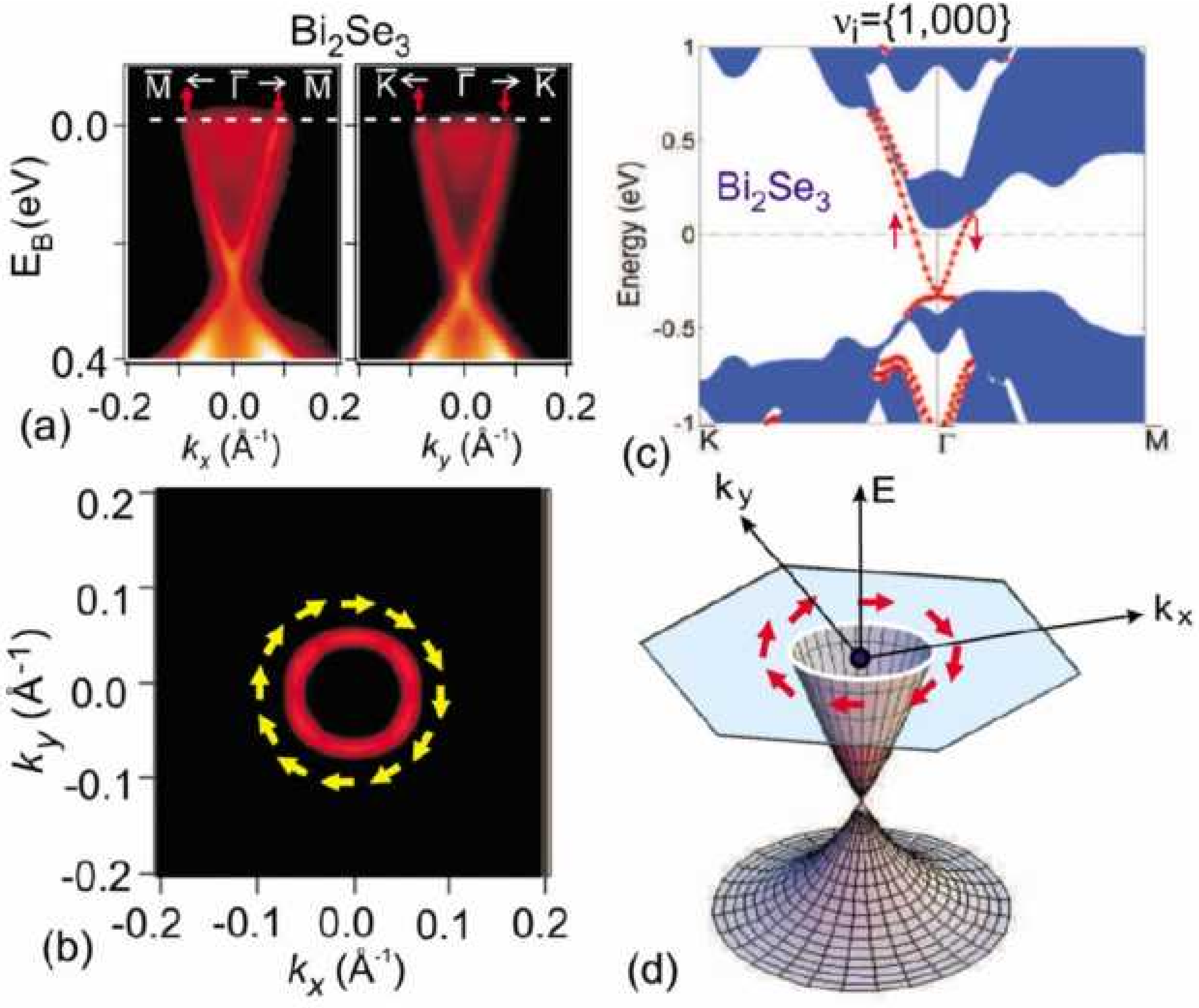

Quantum Spin Hall Effect in HgTe quantum wells

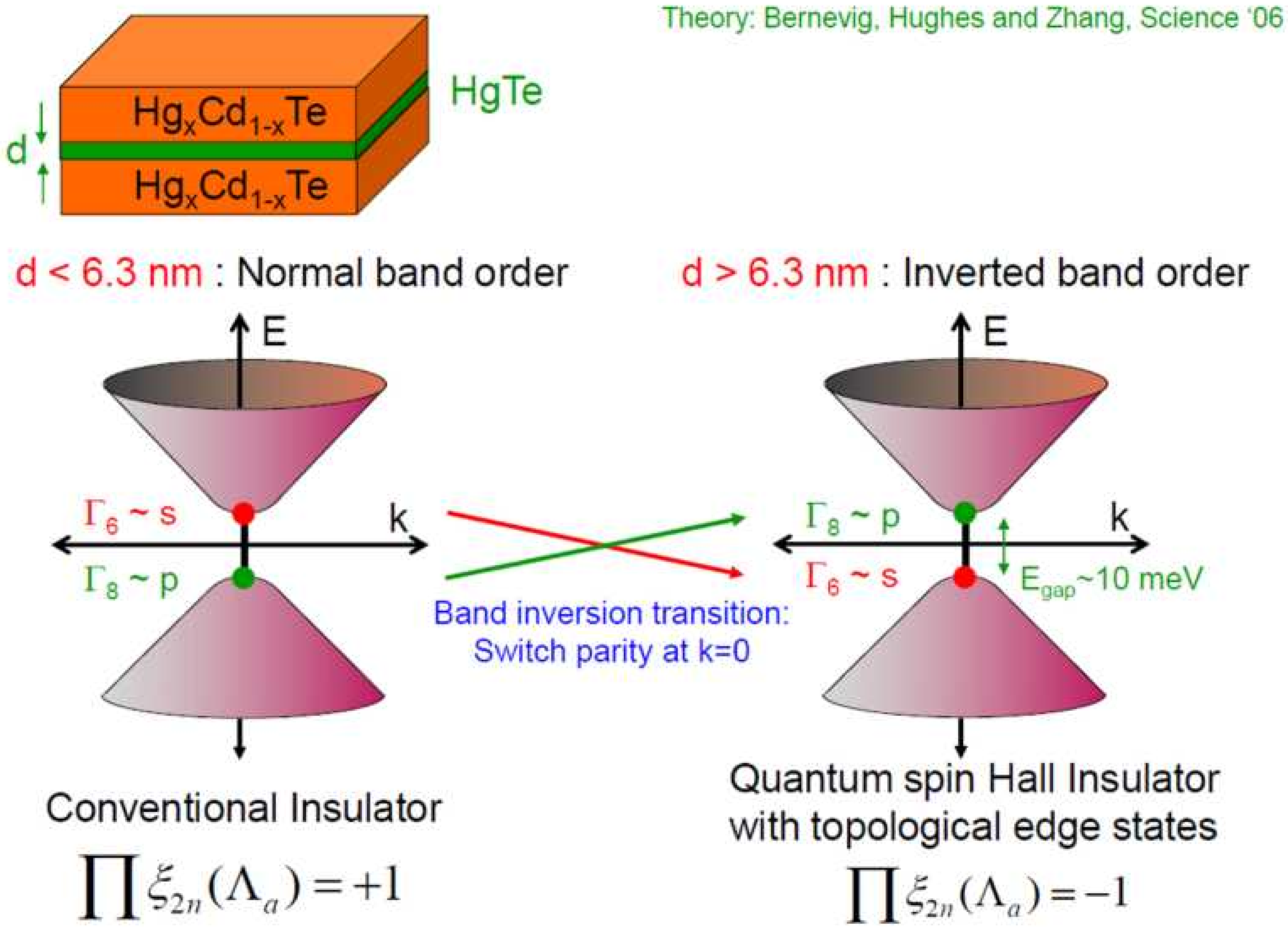

Pankratov, O.A.; Pakhomov, S.V.; Volkov, B.A. (January 1987). "Supersymmetry in heterojunctions: Band-inverting contact on the basis of Pb1-xSnxTe and Hg1-xCdxTe". *Solid State Communications* **61** (2): 93–96

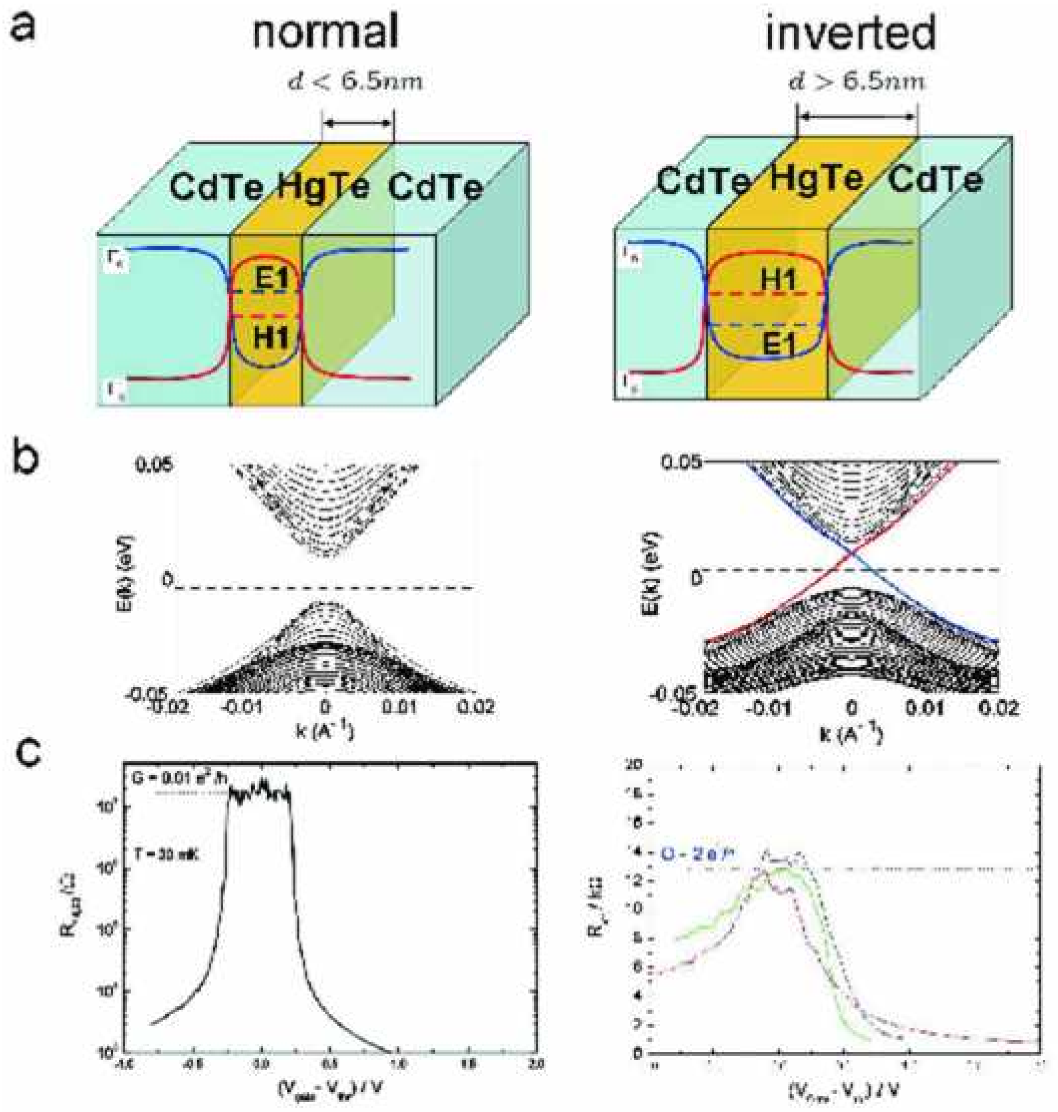

Molenkamp team, Science-2007

Minimal model of Topological Insulator: Dirac Eq. + Boundary Condition

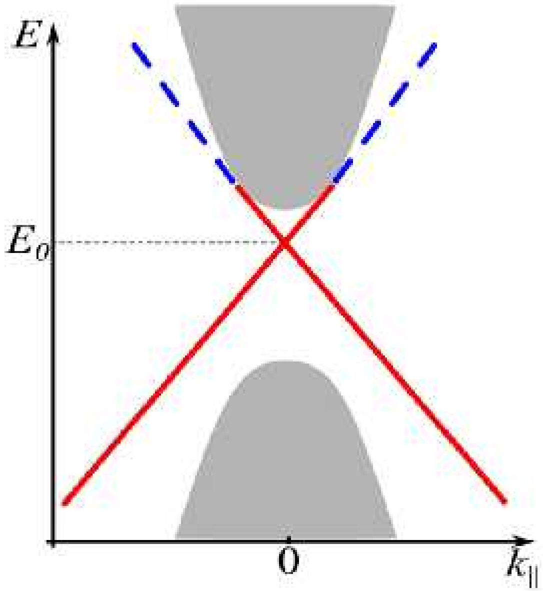

$$\{m\tau_z \otimes \sigma_0 + c\tau_x \otimes (\boldsymbol{\sigma k})\}\,\Psi = E\Psi,$$

$$(\sigma_0 \Psi_v - i a_0 \boldsymbol{\sigma n} \Psi_c)_{\boldsymbol{r}\in S} = 0.$$

σ, τ : Pauli matrices acting in spin and band subspaces,
n = ***n***(*S*) is normal to surface S

Spectrum of 3D Dirac equation (1) in a halfspace with the BC (2).
The sign of a_0 determines whether SSs emerge inside or outside the bulk gap.
$a_0 > 0$: the SSs lie inside the gap – ***topological nontrivial phase***
$a_0 < 0$: the SSs outside the gap – ***trivial phase***.

By means of Dirac Eq. + the BC (2) one may phenomenologically describe the SS in PbSnTe in direct and inverse band order:

V.A. Volkov, T.N. Pinsker, Sov. Phys. Solid State , 23, 1022 (1981).
B.A. Volkov, O.A. Pankratov, JETP Lett., 42, 178 (1985).
B.A. Volkov , B.G. Idlis , M.Sh. Usmanov, Phys. Usp. 38, 761 (1995).

Dirac semi-metals

Topological Dirac semi-metal: 3D graphen-analogue

Bulk 3D massless Dirac fermions in Na_3Bi
Y. Chen et al, Science, 2014

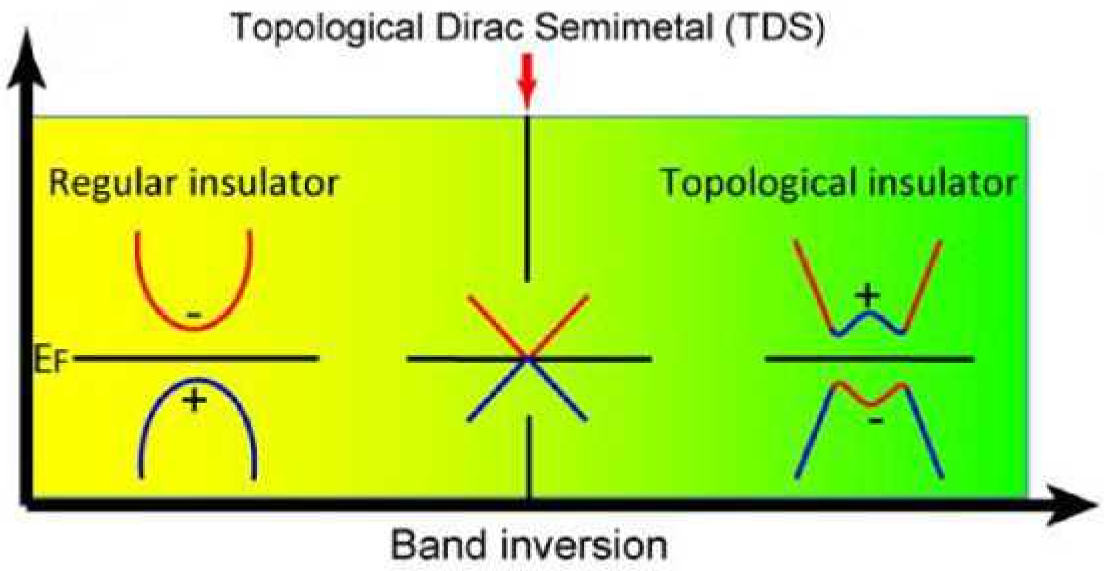

A topological Dirac semi-metal state is realized at the critical point in the phase transition from a normal insulator to a topological insulator. The + and – signs denote the even and odd parity of the energy bands

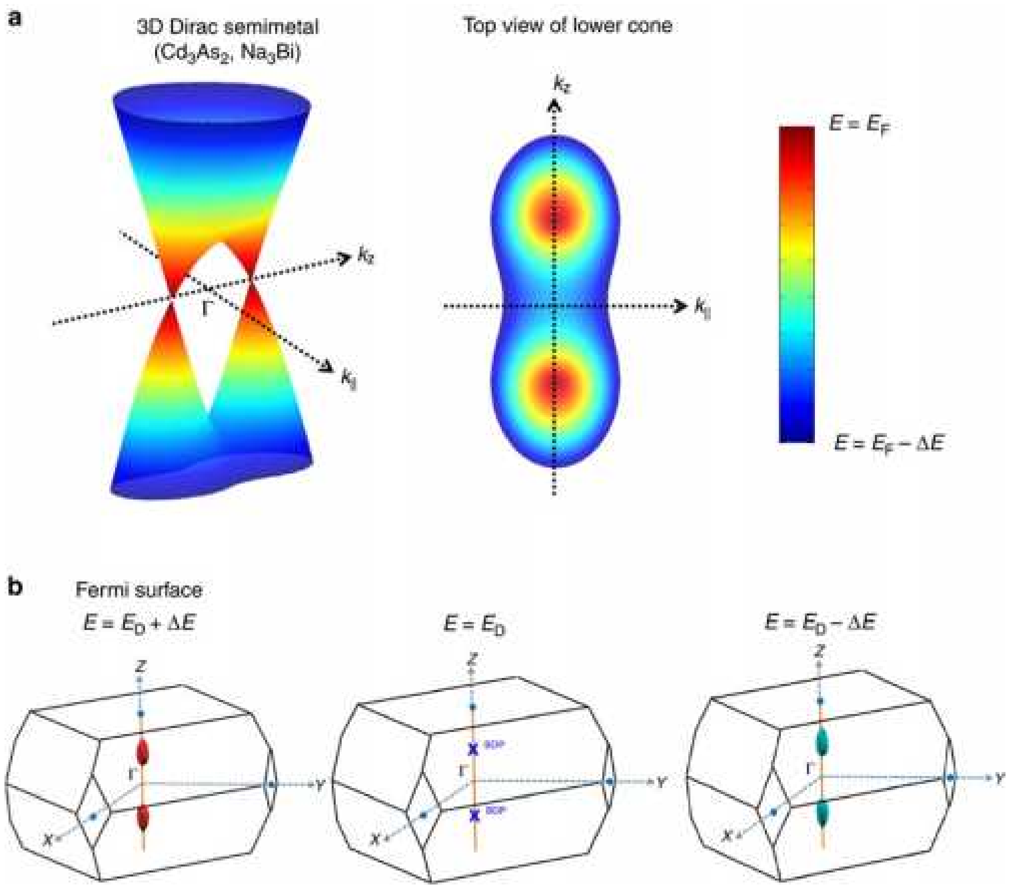

(**a**) Cartoon view of dispersion of 3D Dirac semimetal. (**b**) Schematic view of the Fermi surface above the Dirac point (left panel), at the Dirac point (middle panel) and below the Dirac point (right panel)

Weil semimetals

Surface states in Dirac and Weil semimetals vs TopIns

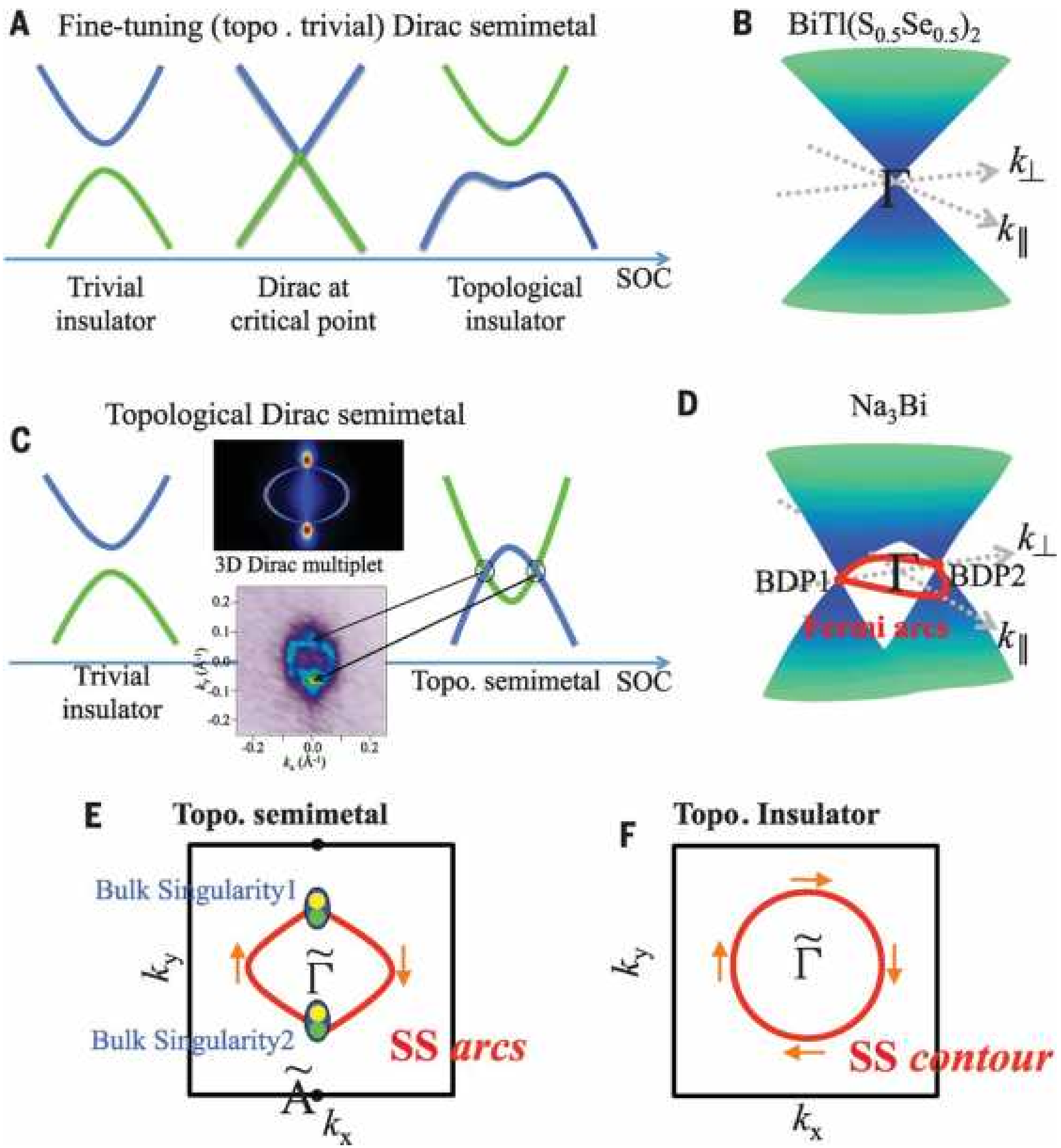

DSM ⇨ WSM

3D topological Dirac semimetals (DSM) in: Na_3Bi and Cd_3As_2
3D Weyl semimetals (WSM) in: monopnictides TX (T=Ta/Nb, X=As/P)

Both classes of materials feature relativistic fermions with linearly dispersing excitations.

WSMs can be seen as evolving from DSMs in the presence of the breaking of time reversal symmetry or space inversion symmetry.

WSMs caused by the loss of space inversion symmetry have been experimentally realized in non-centrosymmetric crystals of TaAs, NbAs, NbP and TaP.

For time reversal symmetry breaking-driven WSM in: $YbMnBi_2$

Weyl semi-metal:

- a 3D analog of graphene;
- crystall where the bulk is gapped except at even number of points in Brillouin zone in which the bands touch (Weyl nodes)

Weyl semimetals: TaAs, NbAs, TaP and NbP

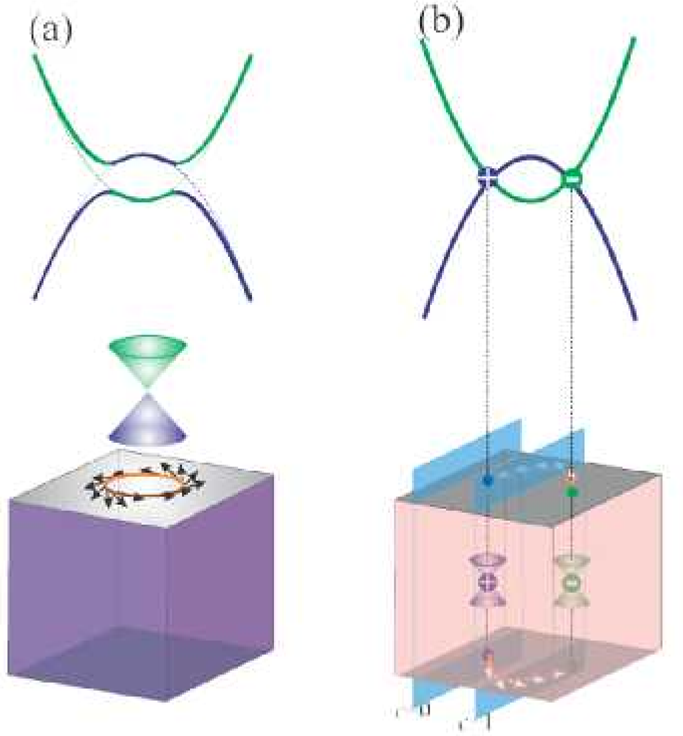

FIG. 1. Schematics of the topological insulator and Weyl semimetal. (a) A TI exhibits an energy gap with a band inversion. Topological surface states exhibits Dirac-cone-type dispersion with spin texture. (b) A WSM is gapless in the bulk and a pair of Weyl points (band crossing points) exists with opposite parity. Nonzero Chern number only exists between negative and positive Weyl points, which leads to a spin-resolved surface Fermi arc.

On surface of Weil semimetal: Fermi arc

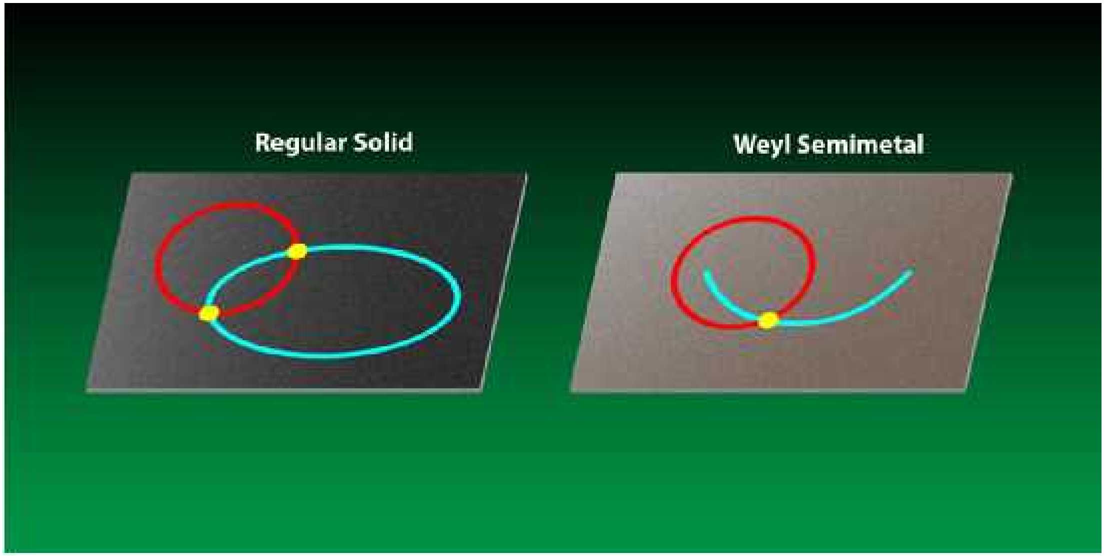

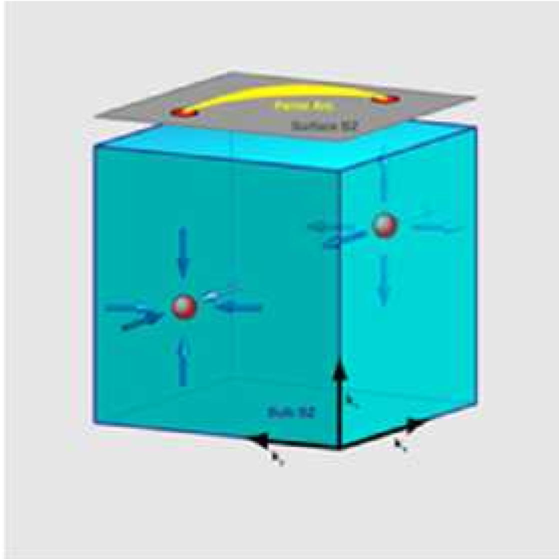

Fig. 1: Two possible Fermi surfaces (blue lines) for momentum states on the outer face of a material. Fermi circle at left represents the usual situation, while the open Fermi arc at right only appears in the context of a Weyl semimetal. The two can be distinguished by counting the number of crossings with an arbitrary closed loop (red). An odd number of crossings can only occur from the Fermi arc

Fig. 2 : A schematic of the Weyl semimetal state, which include the Weyl nodes and the Fermi arcs. The Weyl nodes are momentum space monopoles and anti-monopoles

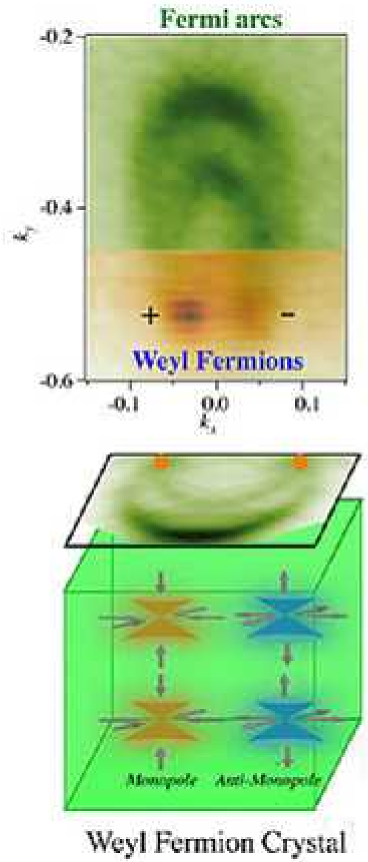

ARPES image (top) signals the existence of Weyl fermion nodes and the Fermi arcs. The plus and minus signs note the particle's chirality. A schematic (bottom) shows the way Weyl fermions inside a crystal can be thought as monopole and antimonopole in momentum space. (Su-Yang Xu and M. Zahid Hasan)

Chiral anomaly
= Adler-Bell-Jackiw anomaly
= axial anomaly

Chiral anomaly (Adler-Bell-Jackiw anomaly, 1969)

plays a key role in the standard model of particle physics.

Hermann Weyl, 1929: massless Dirac equation in 3+1 dimensions can be separated into two two-component equations for Weyl fermions with a definite chirality $\sigma.p$,

$$i\,\frac{\partial\psi}{\partial t} = \pm\, c\, \vec{p}.\vec{\sigma}\, \psi$$

According to the classical equation of motion, the number of fermions with plus or minus chirality is separately conserved. The statement of chiral anomaly is that N_χ, the number of fermion carrying chirality of sign χ is no longer conserved, but obeys the anomaly equation:

$$\frac{dN_\chi}{dt} = \frac{\chi e^2}{4\pi^2\hbar^2 c}(\vec{E}.\vec{B})$$

Explanation (1983, Nielsen and Ninomiya)

1D model: partially filled tight binding band. At the chemical potential we have left and right movers shown in Fig 1 which would appear to be separately conserved if there is no scattering between them. However, in solid state physics these bands are connected far below the Fermi surface and in the presence of an electric field E, the momentum state flows according to the simple equation $\dot{k}$= E. Thus charge flows from left to right as shown in Fig 1, and the number of right movers obey the anomaly equation in 1+1 dimension:

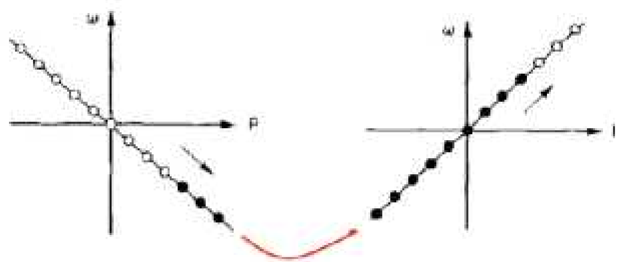

$$\dot{N}_{\mathrm{R}} = \frac{e}{2\pi}\,\mathrm{E}$$

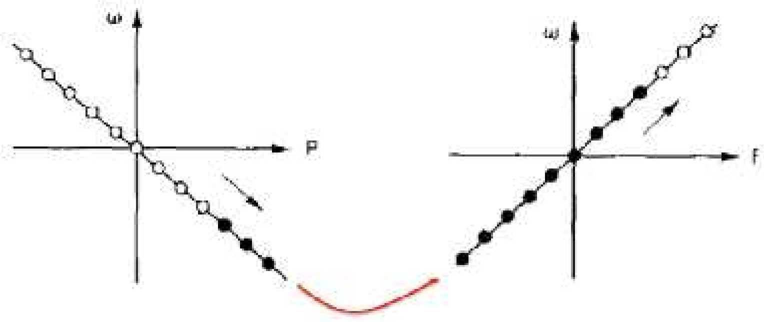

Fig 1. The left and right movers in a one dimensional band are connected far below the Fermi level, allowing charge flow between them. Adapted from Ref. 1.

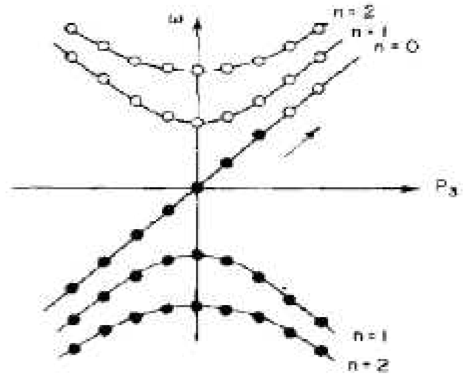

Fig 2. The spectrum vs the z component of the momentum for a 3D Weyl fermion in a magnetic field (From ref 1)

$$\varepsilon_{n,k} = \begin{cases} \frac{\hbar e B}{m_{eff}}(n+\gamma) + \frac{\hbar^2 k_z^2}{2m} & \text{Trivial metal} \\ \hbar v \sqrt{2B(n+\gamma) + k_z^2} & \text{Weyl metal} \end{cases}$$

In usual metals, the quantum correction term γ takes the value ½, but in Weyl systems it attains Berry's phase, such that γ=0.
This is a topological property that depends only on the existence of Weyl nodes and not on the details of the band structure.

Landau levels for Dirac band have a zero energy mode. This mode extends in the pz direction for the 3D Weyl fermion. This band connects the two Weyl nodes serves as the conduit for charge pumping between the two nodes in the presence of an electric field parallel to B. The flow of charge is given by the analog of Eq(3), except that we need to include the degeneracy of the zero mode which is $eB/$ per area normal to B. The right hand side of Eq (3) is then proportional to EzB = $E.B$ and yields exactly Eq(2).

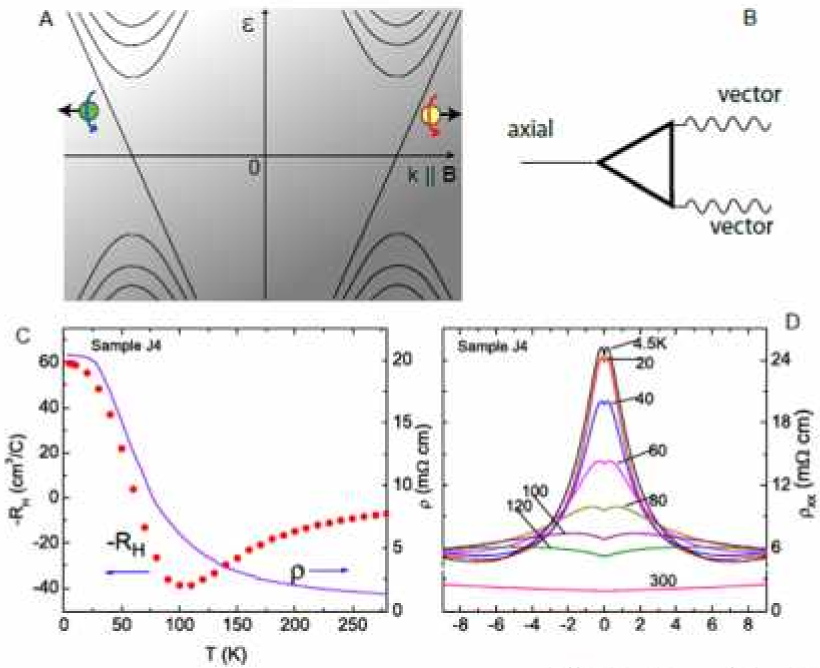

$$\sigma_\chi = \frac{e^2}{4\pi^2\hbar c}\frac{v}{c}\frac{(eBv)^2}{\epsilon_F^2}\tau_v,$$

FIG. 5: Panel A: Sketch of the Landau levels (LL) in a Weyl semimetal showing chiral states in the lowest LL with opposite velocities and chiralities (arrows) $\parallel$ **B**. An **E**-field $\parallel$ **B** breaks chiral symmetry and leads to an axial current. Panel B shows the triangle anomaly that ruins the conservation of chiral charge. Panel C: The T dependence of the resistivity ρ in $B = 0$ and Hall coefficient R_H in Na_3Bi. R_H is measured in B <2 T applied $\parallel$ **c**. At 3 K, R_H corresponds to a density $n = 1.04\times 10^{17}$ cm^{-3}. The inset shows the contact labels and the x and y axes fixed to the sample. Panel D: Curves of the longitudinal magnetoresistance $\rho_{xx}(B,T)$ at selected T from 4.5 to 300 K measured with $\mathbf{B} \parallel \hat{\mathbf{x}}$ and I applied to (1,4). The steep decrease in $\rho_{xx}(B,T)$ at 4.5 K reflects the onset of the axial current in the lowest LL. Adapted from Xiong *et*

ИТОГИ

УПОР на:

<u>Краевые и поверхностные состояния дираковских и вейлевских фермионов</u>

- **Графен** – ***оригинальные результаты***
- **Топологические изоляторы-*обзор***
- **Дираковские полуметаллы-*обзор***
- **Вейлевские полуметаллы-*обзор***
- ***Аксиальная аномалия-обзор***

ПРИЛОЖЕНИЯ

Sciencexpress Reports

Observation of Fermi arc surface states in a topological metal

Su-Yang Xu,[1,2]* Chang Liu,[1]* Satya K. Kushwaha,[3] Raman Sankar,[4] Jason W. Krizan,[3] Ilya Belopolski,[1] Madhab Neupan,e[1] Guang Bian,[1] Nasser Alidoust,[1] Tay-Rong Chang,[5] Horng-Tay Jeng,[5,6] Cheng-Yi Huang,[7] Wei-Feng Tsai,[7] Hsin Lin,[8] Pavel P. Shibayev,[1] Fangcheng Chou,[4] Robert J. Cava,[3] M. Zahid Hasan[1,2]†

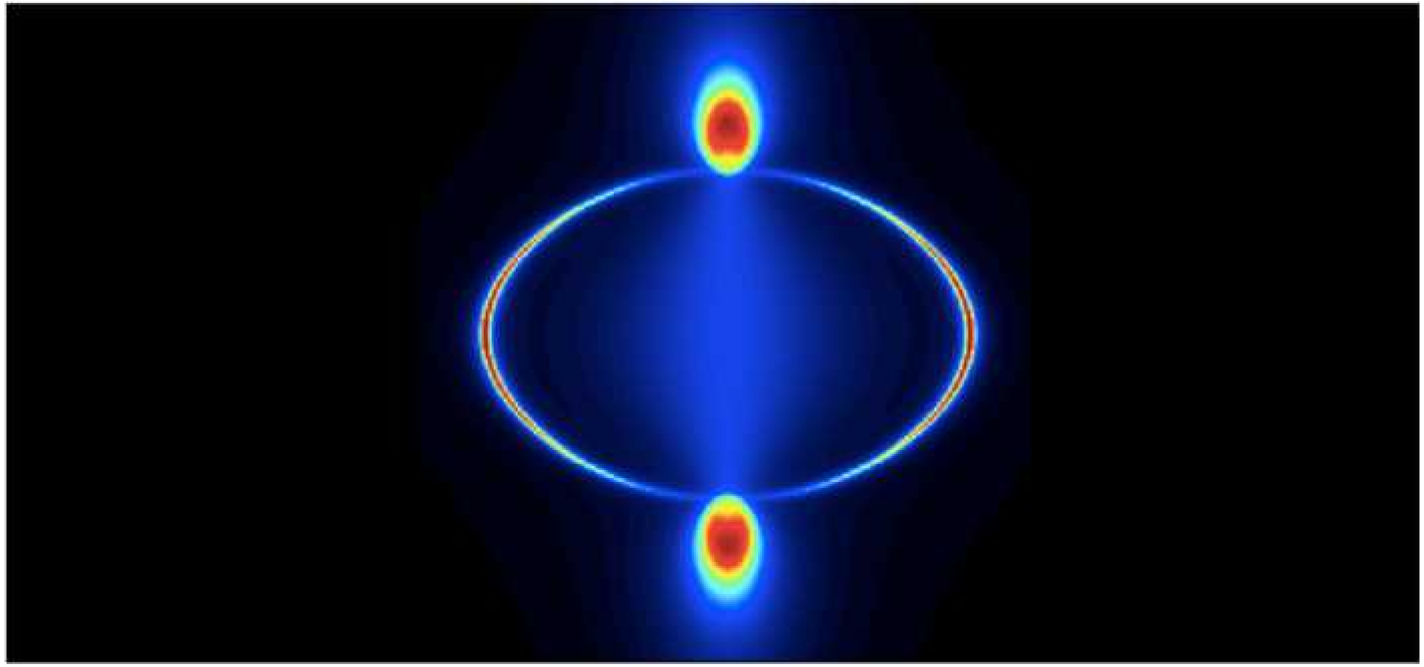

Question: when a 3D Dirac point could be stabilized by space group symmetries in the way that the honeycomb lattice of identical atoms stabilizes graphene's 2D Dirac point?

Effective Hamiltonian of a 2D Dirac point can be taken to be
H = kx!x + ky!y, (1)
whose degeneracy is broken by a perturbation proportional to !z. The most direct generalization of this to 3D is a Weyl point of two bands, such as
H = kx!x + ky!y + kz!z. (2)

This is robust to perturbations, but that robustness results from a topological consideration (a Chern number ±1) which means that there cannot be only one Weyl point on the Fermi surface as the total Chern number must be zero. In materials with both time-reversal and inversion symmetry, Weyl points must come together in pairs and form 3D Dirac points; to see this, note that time-reversal symmetry means that a Weyl point at k must be paired with one at !k with the same Chern number. A center of inversion pairs a Weyl point at k with one with the opposite Chern number at !k. Hence isolated Weyl points are forbidden when both time-reversal and inversion are present. The Hamiltonian at a Dirac point is a 4 by 4 matrix as now four bands are involved. These Dirac points are not topologically protected as their total Chern number is zero, and the question is whether they can be protected by crystalline symmetries. The Dirac semimetals can be a starting point for other states of matter, such as Weyl semimetals if the materials can be modified to break time-reversal or inversion. The chief consequences discussed so far theoretically for Dirac and Weyl semimetals, aside from the band structure probed by ARPES, are in transport. Already transport experiments seeking to observe theoretically predicted anomalies are underway and find high conductivity and large magnetoresistance in single-crystal Cd3As2

Two-band semiconductor with $kp_{cv} \neq 0$: Dirac limit

Narrow-gap 2-band IV-VI or V semiconductors (PbSnTe, PbSnSe or BiSb):

H_{kp} Ĝ H_{cv} , $E_c - E_v = E_{gap}$

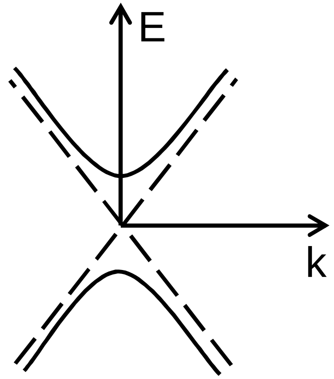

$(E_{gap} \Rightarrow 2mc^2)$

$$H_{cv} = \begin{pmatrix} E_c(0) & \hat{\vec{k}}\vec{p}_{cv} \\ \hat{\vec{k}}\vec{p}_{vc} & E_v(0) \end{pmatrix} \Rightarrow \underbrace{\begin{pmatrix} mc^2 & c\hat{\vec{k}}\hat{\pm} \\ c\hat{\vec{k}}\hat{\pm} & -mc^2 \end{pmatrix}}$$

<u>Dirac Hamiltonian</u> H_D 4x4
for envelope *spinor* $(C_{c\uparrow}, C_{c\downarrow}, C_{v\uparrow}, C_{v\downarrow})$

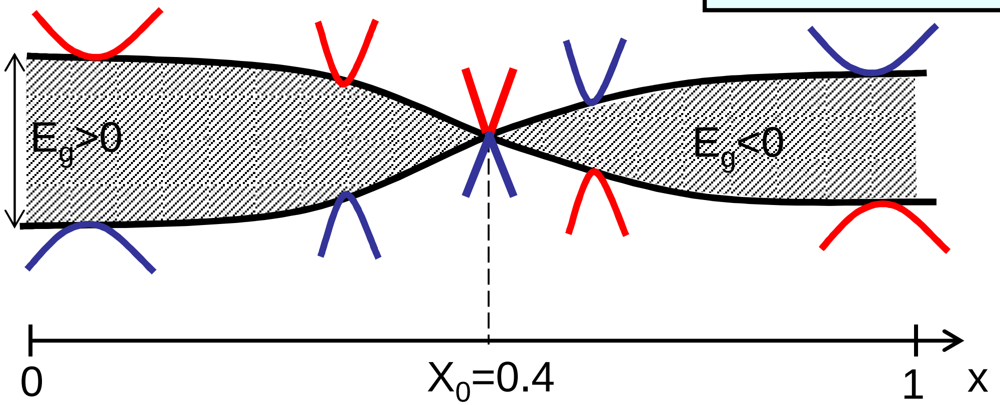

$Pb_xSn_{1-x}Te$

$x=x_0$: accidental <u>gapless state, is not symmetry protected</u>

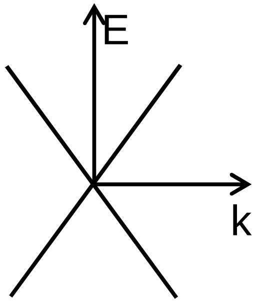

Surface Quantum Hall Effect

Orbital QHE : E=0 Landau Level for Dirac fermions. “Fractional” IQHE

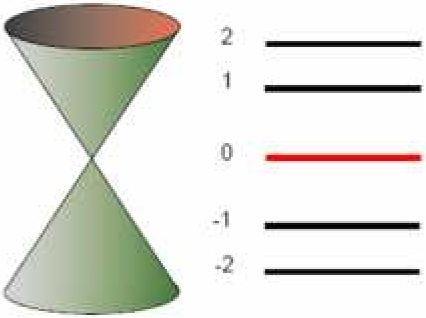

$$\sigma_{xy} = \frac{e^2}{h}\left(n + \frac{1}{2}\right)$$

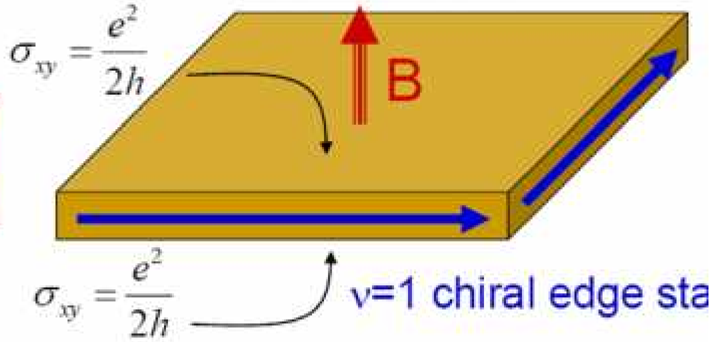

Anomalous QHE : Induce a surface gap by depositing magnetic material

$$H_0 = \psi^\dagger(-i v \vec{\sigma} \cdot \vec{\nabla} - \mu + \Delta_M \sigma_z)\psi$$

Mass due to Exchange field

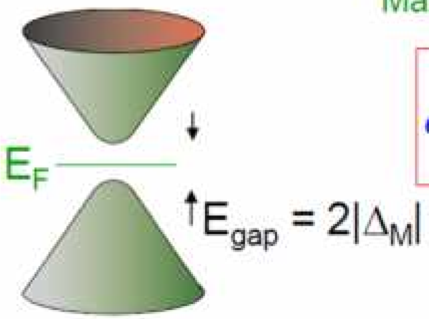

$$\sigma_{xy} = \mathrm{sgn}(\Delta_M)\frac{e^2}{2h}$$

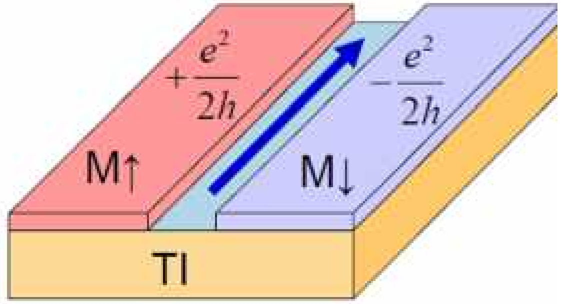

Chiral Edge State at Domain Wall : $\Delta_M \leftrightarrow -\Delta_M$

Time Reversal Symmetry : $[H,\Theta]=0$

Anti Unitary time reversal operator : $\Theta\psi = e^{i\pi S^y/\hbar}\psi^*$

Spin ½ : $\Theta\begin{pmatrix}\psi_\uparrow \\ \psi_\downarrow\end{pmatrix} = \begin{pmatrix}\psi^*_\downarrow \\ -\psi^*_\uparrow\end{pmatrix}$ $\Theta^2 = -1$

Kramers' Theorem: for spin ½ all eigenstates are at least 2 fold degenerate

Proof : for a non degenerate eigenstate $\Theta|\chi\rangle = c|\chi\rangle$, $\Theta^2|\chi\rangle = |c|^2|\chi\rangle$ $\Theta^2 = |c|^2 \neq -1$

Consequences for edge states :

States at "time reversal invariant momenta" k*=0 and k*=π/a (=-π/a) are degenerate.

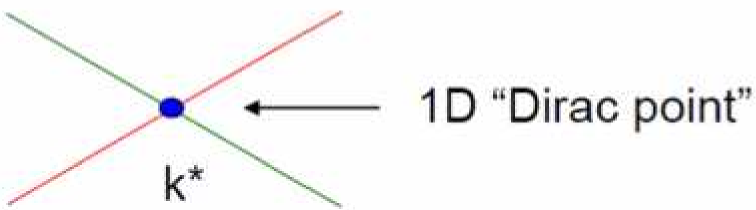

The crossing of the edge states is protected, even if spin conservation is volated.

Absence of backscattering, even for strong disorder. No Anderson localization

Unique Properties of Topological Insulator Surface States

"Half" an ordinary 2DEG ; ¼ Graphene

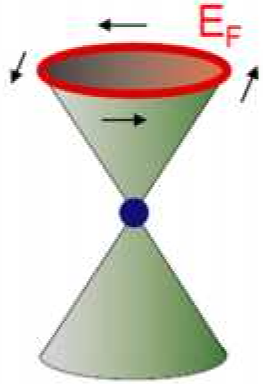

Spin polarized Fermi surface

- Charge Current ~ Spin Density
- Spin Current ~ Charge Density

π Berry's phase

- Robust to disorder
- Weak Antilocalization
- Impossible to localize, Klein paradox

Exotic States when broken symmetry leads to surface energy gap:

- Quantum Hall state, topological magnetoelectric effect

  Fu, Kane '07; Qi, Hughes, Zhang '08, Essin, Moore, Vanderbilt '09

- Superconducting state

  Fu, Kane '08

Концепция топологического изолятора

<u>Википедия:</u> “**Топологический изолятор (ТИ)** — особый тип материала, который внутри объёма представляет собой диэлектрик, а на поверхности проводит электрический ток”.

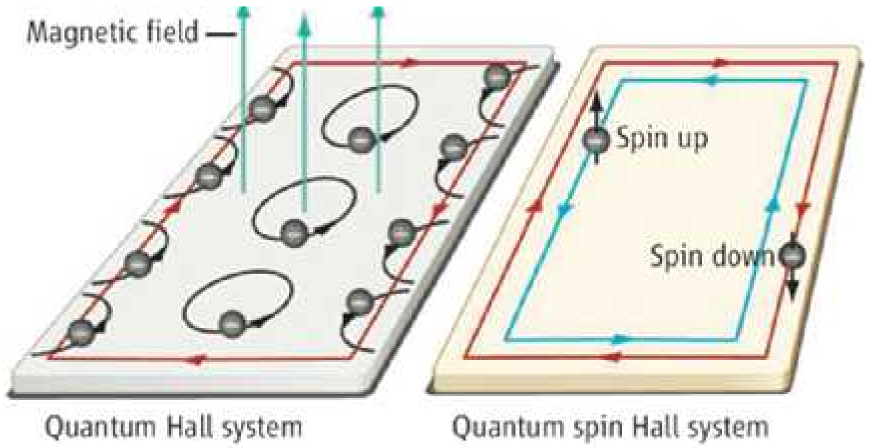

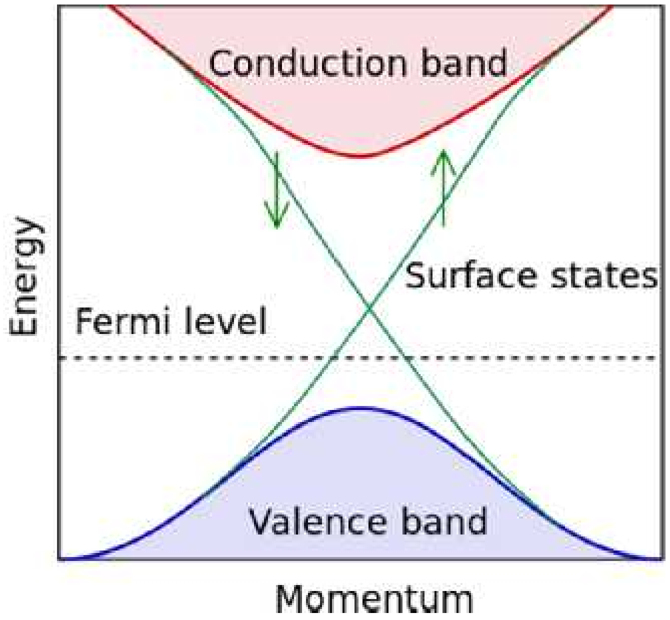

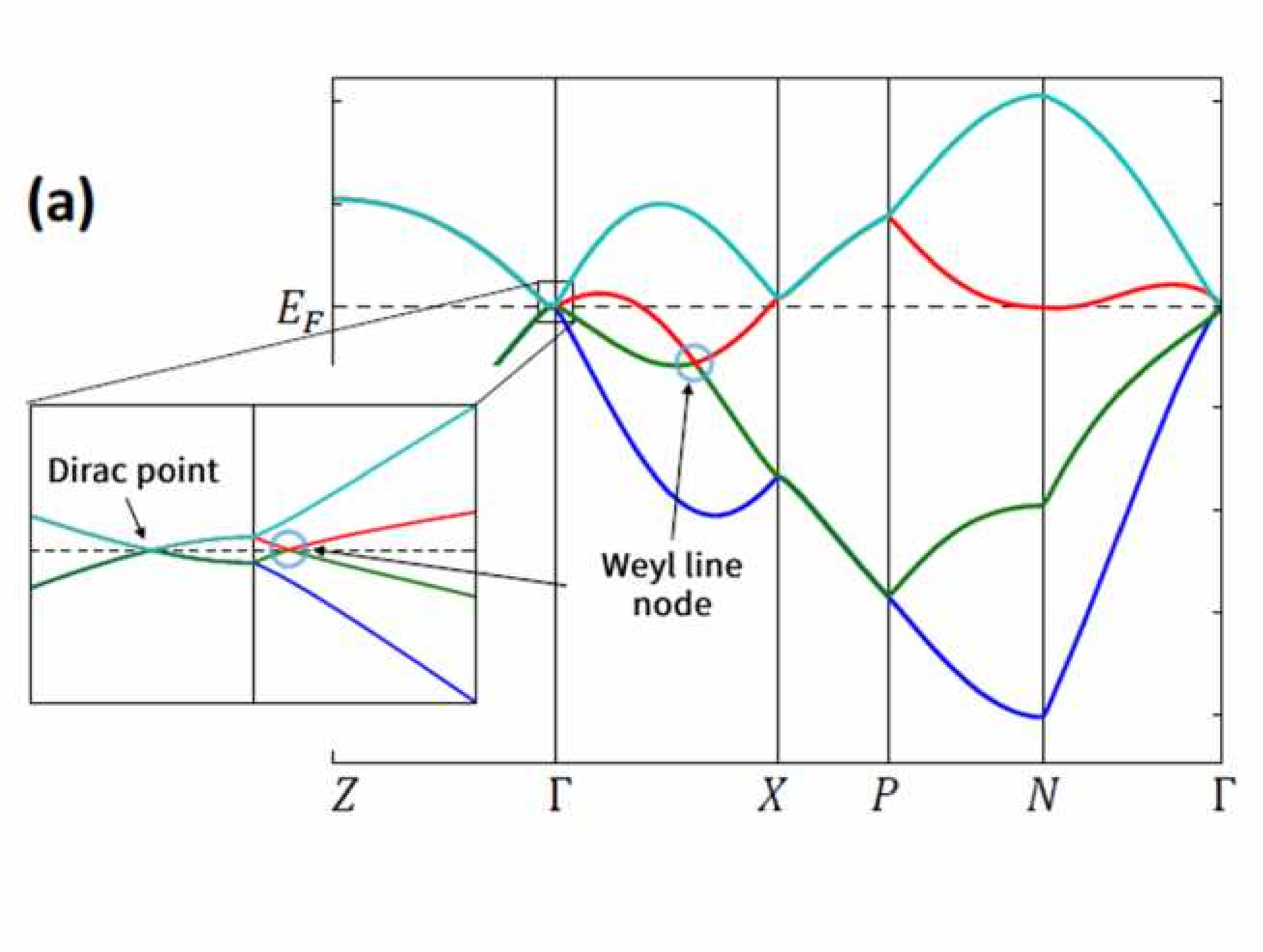

The Dirac points and Weyl line nodes can exist simultaneously.

Experiments on HgCdTe quantum wells

Expt: Konig, Wiedmann, Brune, Roth, Buhmann, Molenkamp, Qi, Zhang Science 2007

d< 6.3 nm
normal band order
conventional insulator

d> 6.3nm
inverted band order
QSH insulator

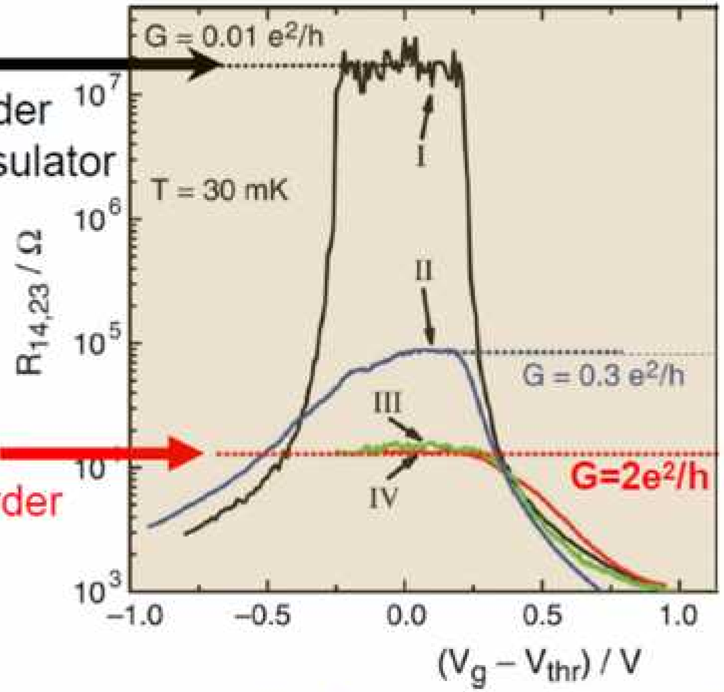

Landauer Conductance G=2e^2/h

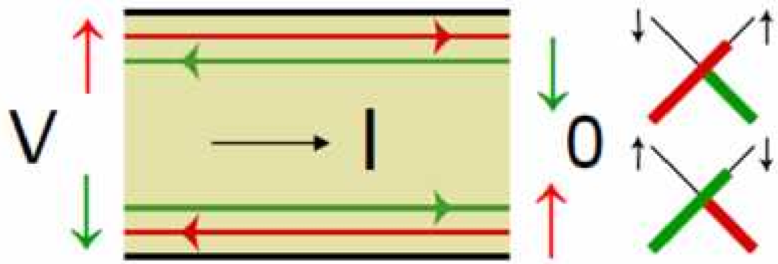

Measured conductance 2e^2/h independent of W for short samples ($L<L_{in}$)

$Bi_{1-x}Sb_x$

Theory: Predict $Bi_{1-x}Sb_x$ is a topological insulator by exploiting inversion symmetry of pure Bi, Sb (Fu,Kane PRL'07)

Experiment: ARPES (Hsieh et al. Nature '08)

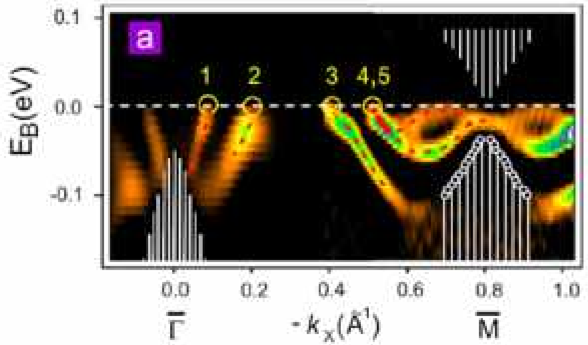

- $Bi_{1-x}Sb_x$ is a Strong Topological Insulator $\nu_0;(\nu_1,\nu_2,\nu_3) = 1;(111)$
- 5 surface state bands cross E_F between Γ and M

Bi_2Se_3

ARPES Experiment : Y. Xia et al., Nature Phys. (2009).
Band Theory : H. Zhang et. al, Nature Phys. (2009).

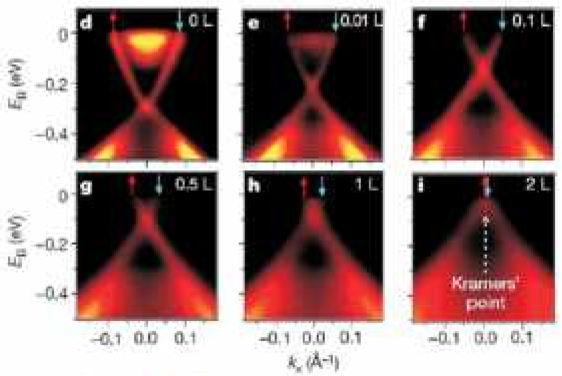

Control E_F on surface by exposing to NO_2

- $\nu_0;(\nu_1,\nu_2,\nu_3) = 1;(000)$: Band inversion at Γ
- Energy gap: $\Delta \sim .3$ eV : A room temperature topological insulator
- Simple surface state structure : Similar to graphene, except only a single Dirac point

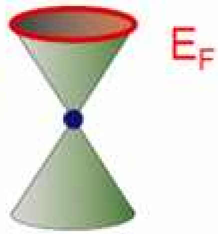

Elemental topological insulator α-Sn:
spin-charge conversion

Rojas-Sánchez et al
Arxiv: Sept 11-2015

Spin to charge conversion
at room temperature

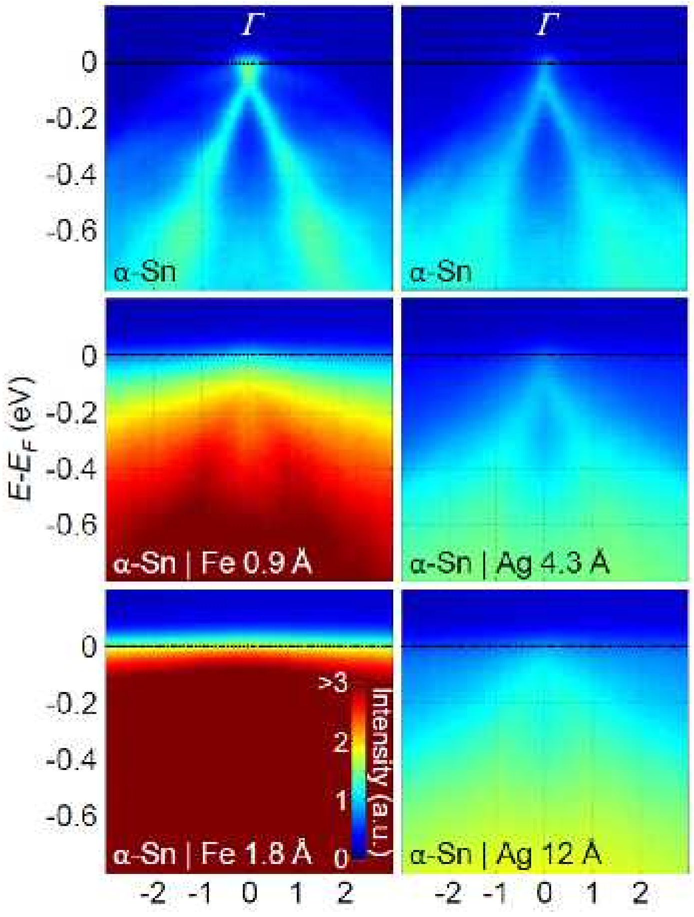

"By ARPES we first confirm that the Dirac cone at the surface of α-Sn (001) layers subsists after covering with Ag".

Weyl semimetals are a topological state of matter in which the conduction and valence bands touch and linearly disperse around pairs of Weyl nodes20,21. Each node has a denite left or right handed chirality providing a quantum number analogous to the valley degree of freedom in graphene22. Dirac semimetals can be thought of as two superimposed copies of Weyl semimetals with the degeneracy protected by a crystal symmetry from opening up a gap4,5,23{25. Similar to topological insulators and their metallic surface, Dirac and Weyl semimetals host protected surface states26
SS only exist for a restricted range of crystal momenta, thereby forming a Fermi arc connecting a pair of Weyl points with opposite chirality26,27. The chiral fermions describing the low energy degrees
of freedom of Dirac and Weyl semimetals exhibit the chiral anomaly28{30: while the sum of left and right handed fermions is necessarily conserved, their dierence, the chiral density, does not have to be, even if classically it should. In fact, non-orthogonal magnetic and electric elds pump left handed fermions into right handed, or vice versa29{34.

Visualization of the chiral anomaly in Dirac and Weyl semimetals

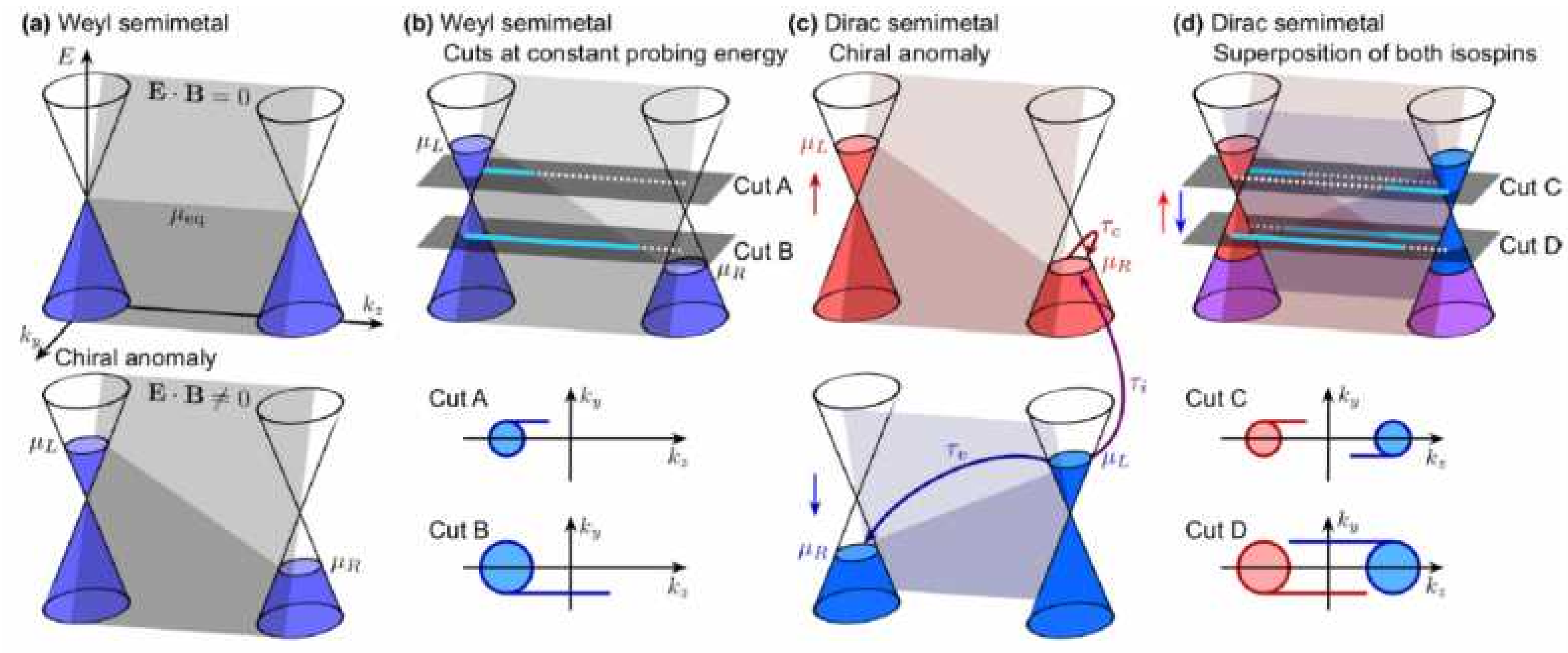

(a) Spectrum of a Weyl semimetal with two bulk Weyl nodes of different chirality separated in momentum space. The grey plane represents the SS at the top surface, occupied up to the equilibrium chemical potential Applying magnetic and electric fields results in a steady state with left and right cone chemical potentials, linearly interpolated by a tilted Fermi arc.

(b) Two constant energy cuts (A and B) through the band structure, with occupied and empty SSs (solid light blue and white dashed lines)

(c) Dirac semimetals host pairs of Weyl cones, each pair with isospin and both left and right chiralities, that respond to the chiral anomaly in the opposite way. Two edge states with opposite velocities (light red and light blue planes), appear at each boundary of the Dirac semimetal. Scattering processes are depicted by arrows.

(d) The two pairs of Weyl nodes in (c) together comprise a pair of Dirac nodes. At energy cuts (C and D) between L and R, both bulk nodes are occupied while SSs are only partially occupied. The total occupation in these planes illustrated in the bottom panel.